Quaternary Geochronology 27 (2015) 33–51

Contents lists available at ScienceDirect

Quaternary Geochronology

journal homepage: www.elsevier.com/locate/quageo

Research paper

Differences in ^{10}Be concentrations between river sand, gravel and pebbles along the western side of the central Andes

S. Carretier [a, *], V. Regard [a], R. Vassallo [f], G. Aguilar [a, g, h], J. Martinod [a, f], R. Riquelme [b], F. Christophoul [a], R. Charrier [c, d], E. Gayer [i], M. Farías [c], L. Audin [e], C. Lagane [a]

[a] Géosciences Environnement Toulouse, OMP, UPS, CNRS, IRD, Université de Toulouse, France
[b] Departamento de Ciencias Geológicas, Facultad de Ingeniería y Ciencias Geológicas, Universidad Católica del Norte, Antofagasta, Chile
[c] Departamento de Geología, Universidad de Chile, Santiago, Chile
[d] Escuela de Ciencias de la Tierra, Universidad Nacional Andres Bello, Campus República, Santiago, Chile
[e] Institut des Sciences de la Terre, CNRS, IRD, Université de Grenoble, France
[f] Université de Savoie, ISTerre, F-73376 Le Bourget du Lac, France
[g] Departamento de Geologia, Universidad de Atacama, Copiapo, Chile
[h] Advanced Mining Technology Center, Facultad de Ciencias Física y Matemática, Univ. de Chile, Chile
[i] Institut de Physique du Globe, Paris, France

ARTICLE INFO

Article history:
Received 14 May 2014
Received in revised form
27 November 2014
Accepted 2 December 2014
Available online 3 December 2014

Keywords:
Andes
Sand
Pebbles
Gravels
Sediment
Cosmogenic nuclide
Erosion
Granulometry

ABSTRACT

Cosmogenic nuclides in river sediment have been used to quantify catchment-mean erosion rates. Nevertheless, variable differences in ^{10}Be concentrations according to grain size have been reported. We analyzed these differences in eleven catchments on the western side of the Andes, covering contrasting climates and slopes. The data include eight sand (0.5–1 mm) and gravel (1–3 cm) pairs and twelve sand (0.5–1 mm) and pebble (5–10 cm) pairs. The difference observed in three pairs can be explained by a difference in the provenance of the sand and coarser sediment. The other sand–pebble pairs show a lower ^{10}Be concentration in the pebbles, except for one pair that shows similar concentrations. Two sand–gravel pairs show a lower ^{10}Be concentration in the gravel and the other five pairs show a higher ^{10}Be concentration in the gravel. Differences in climate do not reveal a particular influence on the ^{10}Be concentration between pairs. The analysis supports a model where pebbles and gravel are mainly derived from catchment areas that are eroding at a faster rate. The five gravel samples with high ^{10}Be concentrations probably contain gravel that were derived from the abrasion of cobbles exhumed at high elevations. In order to validate this model, further work should test if pebbles are preferentially exhumed from high erosion rate areas, and if the difference between pebbles with high ^{10}Be concentrations and sand decreases when the erosion rate tends to be homogeneous within a catchment.

1. Introduction

This paper explores the differences in the mean ^{10}Be content in sand, gravel (1–3 cm) and pebbles (5–10 cm) covering a river bed. The catchment-mean erosion rates were estimated from the mean ^{10}Be concentration in several-hundred grams of a sand sample gathered in a river at a catchment outlet. The ^{10}Be concentration in each sand grain is assumed to correspond to the ^{10}Be production on the hillside during stationary exhumation only. It is assumed that the thousands of grains found within a sand sample come from everywhere in the catchment, meaning that their mean ^{10}Be concentration provides information about the mean catchment erosion rate (e.g. Brown et al., 1995; Granger et al., 1996; Bierman and Steig, 1996; von Blanckenburg, 2005). This method could be improved by separating clasts coming from different lithological sources. This would allow us to determine the erosion rate of different patches, opening the way to mapping erosion rates in different areas of large and inaccessible catchments by sampling river bed material at its outlet. More generally, the sampling of sediment deriving from a specified source may improve our understanding of hillslope and river erosion processes (e.g. Codilean et al., 2010; Gayer et al., 2008; Nichols et al., 2002; Matmon et al., 2013; Carretier and Regard, 2011). These approaches require the sampling of clasts that are large enough (>1 cm) in order to identify the selected lithology.

* Corresponding author.
E-mail address: sebastien.carretier@get.obs-mip.fr (S. Carretier).

http://dx.doi.org/10.1016/j.quageo.2014.12.002
1871-1014/

Nevertheless, ^{10}Be acquisition in coarse sediment such as this can be different from that of sand. Previous studies have shown either a positive correlation between the grain size and ^{10}Be concentration (Belmont et al., 2007; Clapp et al., 2002; Heimsath et al., 2010; Hewawasam et al., 2003; Matmon et al., 2005b; Reinhardt et al., 2007; Ouimet et al., 2009; Wittmann et al., 2007, 2011b, 2011c, see the compilation in the supplementary information provided by Codilean et al., 2014), a negative correlation (Aguilar et al., 2014; Belmont et al., 2007; Brown et al., 1995, 1998; Codilean et al., 2014; Derrieux et al., 2014; Insel et al., 2010; Oskin et al., 2008; Matmon et al., 2003; Palumbo et al., 2010; Puchol et al., 2014; Reinhardt et al., 2007; Wittmann et al., 2007, 2009, 2011b, 2011c), or similar ^{10}Be concentrations in the different grain size fractions (Binnie et al., 2006; Clapp et al., 2000, 2001, 2002; Granger et al., 1996; Kober et al., 2009; Norton et al., 2008, 2011; Palumbo et al., 2010; Schaller et al., 2001; Stock et al., 2009; Wittmann et al., 2011b,c). Different explanations have been given for these differences or similarities, involving hillslope and river processes, which are detailed in the next section. However, the differences in grain size, climatic environment and slope analyzed in the different studies make it difficult to compare them (e.g. Brown et al., 1995; Belmont et al., 2007). The variations in cosmogenic nuclide concentrations between the different grain sizes is probably linked to differences in the rate of the hillslope and river processes (Bierman and Nichols, 2004), but this link still needs to be established.

In this paper, we analyze the relationships between the ^{10}Be concentration and sediment size in the Andean catchments of southern Perú and central Chile, covering a wide range of climates, drainage areas, slopes and erosion rates. We separate the studied grain sizes into three fractions, called sand (0.5–1 mm), gravel (1–3 cm) and pebbles (5–10 cm). We are studying these coarse fractions because we hypothesize that larger and systematic differences in the ^{10}Be concentration may emerge from larger differences in the grain size. We assume that by comparing the same fractions in different climatic contexts, it will help to better understand the relative role of climate, landslides, provenance and erosion rates on the grain size dependence of the ^{10}Be concentration. The 37 ^{10}Be concentrations presented here include 15 ^{10}Be concentrations in sand first published by Carretier et al. (2013) and four ^{10}Be concentrations in the coarse fraction from the Huasco catchment first published by Aguilar et al. (2014) (Table 1). In this contribution, we first report the literature on this topic, then we describe the regional context, sampling procedure and geomorphic parameters used to compare the catchments. Then we present the differences in ^{10}Be concentrations between the different grain sizes, and we discuss the possible explanations for these differences, based on previous studies.

2. Previous works on grain size dependence

Previous authors have given different interpretations of the observed difference or absence of grain size dependence, as

Table 1
Details about the ^{10}Be measurements and samples. Sample names with stars were prepared at the GET Toulouse laboratory, all others were prepared at Cerege, Aix en Provence. The sample names with † are from Aguilar et al. (2014). Sample names with ‡ are from Carretier et al. (2013).

Lat.	Long.	Name	Size	Number of clasts	Mass of quartz (g)	^{10}Be/^{9}Be	±σ	^{10}Be (atoms/g)	±σ
−13.0275	−76.1932	CAN2	[0.5–1] mm	>1000	24.18	4.03E-13	2.54E-14	3.28E+05	2.07E+04
−13.0275	−76.1932	CAN3	[5–10] cm	6	46.46	1.02E-13	1.49E-014	5.27E+04	7.8E+03
−16.3476	−73.1344	OCO22	[0.5–1] mm	>1000	46.13	1.90E-13	2.35E-014	9.95E+04	1.26E+04
−16.3476	−73.1344	OCO24	[5–10] cm	15	61.77	1.86E-14	3.08E-015	7.35E+03	1.2E+03
−16.3476	−73.1344	OCO25	[1–3] cm	31	31.84	5.04E-014	3.10E-015	3.23E+04	2.2E+03
−28.9911	−70.2782	HUA1‡	[0.5–1] mm	>1000	34.25	8.08E-013	2.28E-014	4.80E+05	1.4E+04
−28.9911	−70.2782	HUA3†	[5–10] cm	15	13.32	1.86E-013	8.26E-015	3.32E+05	1.8E+04
−28.5995	−70.7277	HUA12‡	[0.5–1] mm	>1000	49.52	1.24E-012	3.60E-014	5.99E+05	2.5E+04
−28.5995	−70.7277	HUA14†	[5–10] cm	30	14.69	1.53E-013	6.13E-015	2.49E+05	1.2E+04
−28.7031	−70.5512	HUA10‡	[0.5–1] mm	>1000	37.35	1.08E-012	3.03E-014	5.89E+05	1.7E+04
−28.7031	−70.5512	HUA11†	[5–10] cm	30	10.13	9.15E-014	7.43E-015	2.16E+05	1.9E+04
−28.7978	−70.4579	HUA7‡	[0.5–1] mm	>1000	16.71	6.91E-013	4.43E-014	8.33E+05	5.4E+04
−28.7978	−70.4579	HUA9†	[1–3] cm	34	20.43	3.18E-013	2.41E-014	3.19E+05	2.7E+04
−29.8477	−70.4938	ELK1‡	[0.5–1] mm	>1000	41.98	3.09E-013	3.97E-014	1.77E+05	2.3E+04
−29.8477	−70.4938	ELK2‡	[0.5–1] mm	>1000	16.21	1.49E-013	1.21E-014	1.87E+05	1.7E+04
−29.8477	−70.4938	ELK3	[5–10] cm	30	14.12	9.72E-014	8.62E-015	1.38E+05	1.2E+04
−29.8477	−70.4938	ELK5	[1–3] cm	40	21.69	3.99E-013	3.21E-014	3.71E+05	3.0E+04
−31.5999	−71.1131	ILL1‡	[0.5–1] mm	>1000	18.87	4.36E-013	1.24E-014	4.69E+05	1.3E+04
−31.5999	−71.1131	ILL3	[1–3] cm	30	20.45	7.82E-013	6.50E-014	7.68E+05	6.4E+04
−31.5971	−71.4045	CHO0823S‡	[0.5–1] mm	>1000	15.45	1.67E-013	6.98E-015	2.18E+05	9.5E+03
−31.5971	−71.4045	CHO0823G	[5–10] cm	30	33.91	3.91E-013	1.24E-014	2.34E+05	7.8E+03
−31.6628	−71.3000	CHO0822S‡	[0.5–1] mm	>1000	35.38	3.47E-013	9.91E-015	1.98E+05	5.8E+03
−31.6628	−71.3000	CHO0822G	[5–10] cm	30	32.62	1.60E-013	9.34E-015	9.85E+04	5.8E+03
−31.6921	−71.2677	CHO1‡	[0.5–1] mm	>1000	23.02	2.22E-013	7.52E-015	1.96E+05	6.7E+03
−31.6921	−71.2677	CHO2	[5–10] cm	30	36.99	1.46E-013	5.67E-015	7.95E+04	3.1E+03
−31.6921	−71.2677	CHO3	[1–3] cm	100	22.16	4.62E-013	4.17E-014	4.21E+05	3.8E+04
−32.8349	−70.5449	ACO1‡	[0.5–1] mm	>1000	40.11	1.72E-013	2.13E-014	1.01E+05	2.9E+03
−32.8349	−70.5449	ACO3	[1–3] cm	100	26.79	2.56E-013	2.48E-014	1.94E+05	1.9E+04
−34.6767	−70.8713	TIN1‡	[0.5–1] mm	>1000	32.58	1.60E-013	8.42E-015	9.94E+04	5.3E+03
−34.6767	−70.8713	TIN2	[1–3] cm	100	22.64	1.88E-013	1.56E-014	1.77E+05	1.7E+04
−34.6767	−70.8713	TIN3	[5–10] cm	30	27.64	1.02E-013	1.68E-014	7.39E+04	1.35E+04
−34.9863	−70.8649	TEN1‡	[0.5–1] mm	>1000	0.47	2.82E-015	8.91E-016	7.33E+04	4.81E+04
−34.9863	−70.8649	TEN3	[1–3] cm	100	25.55	1.45E-014	1.61E-015	1.06E+04	1.4E+03
−35.1844	−71.1161	LON1‡	[0.5–1] mm	>1000	1.02	4.37E-015	1.26E-015	6.44E+04	2.91E+04
−35.1844	−71.1161	LON2	[1–3] cm	100	18.35	4.24E-014	1.06E-014	4.66E+04	1.17E+04
−35.7274	−71.0209	MAU1‡	[0.5–1] mm	>1000	44.54	2.40E-013	2.65E-014	1.29E+05	1.5E+04
−35.7274	−71.0209	MAU3	[5–10] cm	30	26.63	1.77E-014	3.13E-015	1.26E+04	2.5E+03

illustrated by Fig. 1. In their pioneer study in Puerto Rican catchments, Brown et al. (1995) showed that the coarsest sediment (~8 mm) has a lower ^{10}Be concentration than the smaller grains because they are mainly derived from depth during landslides (Fig. 1A). This interpretation is strongly supported by the similar ^{10}Be concentration in coarse sediment and that of gravel-sized saprolite material found at depths of 1.5–2 m and affected by mass wasting (Brown et al., 1995). Belmont et al. (2007), in the Clearwater River, western Washington state, Aguilar et al. (2014) in the arid Huasco catchment in the Chilean Andes, and Puchol et al. (2014) in central Himalayas proposed a similar explanation for the smaller mean ^{10}Be concentration in larger pebbles compared to that of sand (0.5–1 mm). Aguilar et al. (2014) proposed that the difference in the ^{10}Be concentration between these larger pebbles and sand may be used to quantify the mean erosion rate of catchment areas dominated by landslides (Fig. 1A). The lack of grain size dependence in low-slope rivers and in arid catchments (e.g. Clapp et al., 2000, 2001, 2002; Granger et al., 1996; Schaller et al., 2001) seems to be consistent with the minor role of mass wasting in these catchments: for example, Clapp et al. (2001) proposed that in a

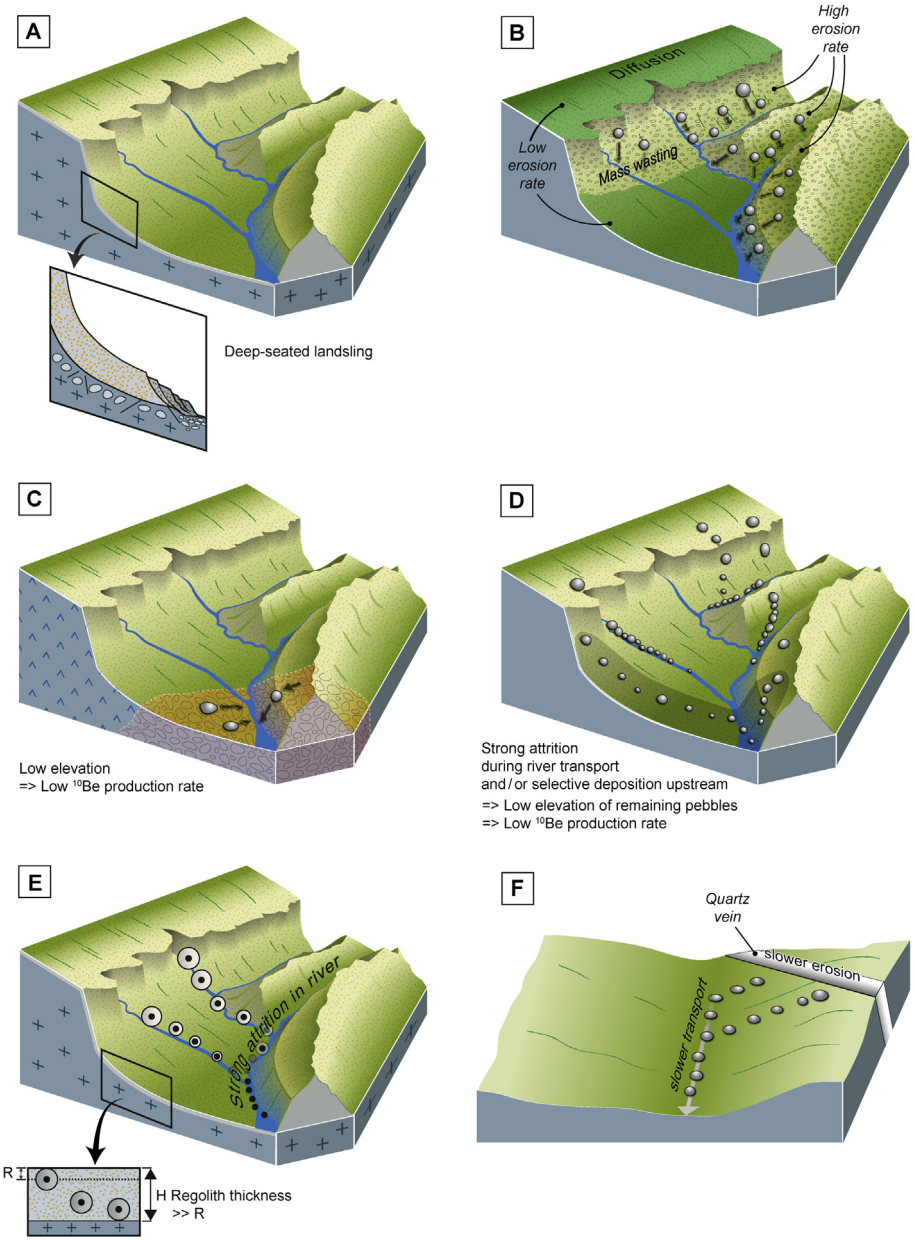

Fig. 1. Different scenarios that could produce differences in the ^{10}Be concentrations between sand, gravel and pebbles. A – Landslides exhume coarse sediment with a lower ^{10}Be concentration (e.g. Brown et al., 1995; Puchol et al., 2014). B – Coarse sediment are preferentially produced on steep slopes that are eroding faster, resulting in a lower ^{10}Be concentration than sand (e.g. Belmont et al., 2007; Aguilar et al., 2014). C – Coarse sediment comes from a lithology present only at low elevations, resulting in a lower ^{10}Be concentration than that of sand (e.g. Matmon et al., 2003). D – Pebbles or gravel come from low elevations, either because of selective deposition upstream of more distant clasts (e.g. Wittmann et al., 2011c), or because their size reduction by attrition is such that the distant pebbles have been entirely crushed (e.g. Carretier et al., 2009). This results in a lower ^{10}Be concentration in the pebbles. On the other hand, this process can decrease the ^{10}Be concentration in fine sand (dilution) if the distant pebbles had lower ^{10}Be concentration than the sand on the hillslopes (e.g. Belmont et al., 2007). E – If the mobile soil is very thick, and if the pebbles are derived from the attrition of boulders, then their mean ^{10}Be concentration is lower than that of sand (e.g. Aguilar et al., 2014). F – On gentle slopes, pebbles eroded from a resistant lithology, and then moving slowly in the river, have a larger ^{10}Be concentration than sand (Codilean et al., 2014).

semi-arid catchment located at the southern edge of the Colorado plateau, sediment of different sizes moves at the same velocity on the hillslope and differential transport in rivers dominated by flash-floods is less likely. Nevertheless, the data given by Reinhardt et al. (2007) for a catchment in southern Spain do not fully support this interpretation. In the steep (25–90°) and fast eroding part of this catchment, dominated by mass wasting, two river sediment samples show smaller ^{10}Be concentrations in the [8–16] mm size fraction compared to the [0.25–5] mm size fraction, but another sample shows the reverse. Furthermore, in the low slope (<25°) upper part of the catchment, the [8–16] mm size fraction has a ^{10}Be concentration that is 1.5 times higher than the [0.25–5] mm size fraction, which is different from what Clapp et al. (2000) observed in their arid and low slope catchments. The lack of sediment mixing in this relatively small catchment (~20 km^2) may explain the variable ^{10}Be concentrations (Binnie et al., 2006; Niemi et al., 2005; Yanites et al., 2009). Nevertheless, the size of the catchments studied by Reinhardt et al. (2007) is either the same size or larger than the catchments studied by Brown et al. (1995), who observed clear differences among the grain sizes. Palumbo et al. (2010) observed the same phenomenon in two mountain ranges in the Qilian Shan foreland (NE-Tibet). They obtained a higher ^{10}Be concentration in three sand samples (0.2-0-71 mm) compared to gravel samples (2–20 cm) in three small catchments (0.79–8.43 km^2), with a mean slope angle ranging between 14.3° and 28.1°. Another catchment area (2.84 km^2 and with a mean slope angle of 19°) showed the reverse, with a slightly lower mean ^{10}Be concentration in the sand samples compared to the gravel samples. Again, incomplete mixing in these small catchments may explain the observed variability. Nevertheless, Vanacker et al. (2007a,b) in the Ecuadorian Andes, Wittmann et al. (2007) and Norton et al. (2008) in the Alps and Ouimet et al. (2009) in eastern Tibet obtained no or only small differences between the grain sizes in steep catchments. Grain size dependence in these steep catchments is different from what has been observed in other steep catchments with a significant mass wasting imprint (Aguilar et al., 2014; Brown et al., 1995; Belmont et al., 2007; Puchol et al., 2014), making the precise role of landslides unclear for the different grain size fractions. It may be hypothesized that the efficiency of landslides to produce significant differences between ^{10}Be concentrations in coarse and fine sediment should result in a correlation with catchment steepness. However, we do not systematically observe a lower ^{10}Be concentration in coarse sediments for the steeper catchments (Fig. 2B and C), as could be expected if coarse sediment was always exhumed from the deep soil layers by landslides. Furthermore, it may be hypothesized that the differences associated with landslides may depend on the climate, which controls the depth of the soils and thus the depth of the landslides (e.g. Puchol et al., 2014). A possible effect of climate is illustrated by Fig. 2D (precipitation) and E (temperatures). Wetter and colder catchments exhibit a larger variability in the ^{10}Be concentration ratio (higher or lower than 1) between coarse and fine sediments. There are more samples with a lower ^{10}Be concentration in coarse sediment in wet catchments than in arid catchments, which may be consistent with the development of thicker soils under wet climates.

In a steep catchment covered by vegetation in the Great Smoky Mountains (North Carolina and Tennessee), Matmon et al. (2003) also observed a smaller ^{10}Be concentration in coarse sediment (>2 mm and >10 mm) compared to finer sediment. In this case, the coarser sediment are derived from low elevations (low ^{10}Be production rates) which explains the observed difference (Fig. 1C).

Wittmann et al. (2011b) analyzed different size fractions in the [0.125–0.8] mm range among ~50 samples from the Amazon catchment. They observed no difference upstream the confluence between the Negro and Solimões Rivers (north-western part of the Amazon basin), but significant differences were observed downstream between the fine and coarse (>0.5 mm) fractions. Samples that include Andean sources show a higher ^{10}Be concentration in the coarse fraction. Samples that only include slowly eroding cratonic sources show the reverse trend. By analyzing the mean ^{26}Al/^{10}Be ratio of the two grain sizes, Wittmann et al. (2011c) were able to demonstrate that fine sediments have a ratio close to that of Andean sources, with little burial signature, while coarser sediment downstream from the confluence of the Negro and Solimões Rivers are mostly derived from low elevations in the Brazilian shields (low cosmogenic production rate), with a lower ^{26}Al/^{10}Be ratio showing a more pronounced burial signature. In this huge basin, Wittmann et al. (2011b, 2011c) concluded that cosmogenic nuclide differences between the grain size fractions are explained by differences in the provenances and by grain-size selective deposition along the river (Fig. 1D). In addition, this study shows that in a large basin in a low slope cratonic region, coarse sediment present in the river is not necessarily derived from rapidly eroding hillslopes affected by landslides.

Other authors looked at river processes to explain the smaller ^{10}Be concentration in large pebbles. Aguilar et al. (2014) discussed the effect of size reduction during the river transport of initially large boulders buried in deep regolith on the hillslopes, which can produce pebbles with lower ^{10}Be concentrations than sand on average (Fig. 1E). In practice, it is difficult to test for this possibility because the regolith thickness is usually not known in a catchment. Another possibility is that the size reduction in rivers is so efficient that pebbles found at the catchment outlet are only sourced from low elevations, while pebbles produced at the catchment head have been entirely crushed (Fig. 1D). The same cobble size reduction process has been explained by Belmont et al. (2007), but these authors explain the reverse, namely that the mean ^{10}Be concentration in pebbles is higher than that of sand in the downstream part of Clearwater River, in western Washington state. They proposed that a significant fraction of sand comes from the abrasion of cobbles with low ^{10}Be concentrations from the catchment head, which themselves are injected into the river by deep-seated landslides. According to this dilution mechanism, it is this ^{10}Be concentration in sand that is decreased compared to the mean ^{10}Be concentration in pebbles. Belmont et al. (2007) also suggested the possibility that a recent rapid erosion of the hillslopes has exposed sand with a lower ^{10}Be concentration, and which is now being found in the river.

A recent study also shows a higher mean ^{10}Be concentration in pebbles, but for a different reason. Codilean et al. (2014) observed that the mean ^{10}Be and ^{26}Al concentrations in 15 amalgamated pebbles were ten times larger than those of sand at the outlet of the Gaub catchment in Namibia. In this slowly eroding and low slope catchment (~9 m/Ma), Codilean et al. (2014) observed that pebbles were detached from resistant quartz veins. A longer residence time on the hillslopes and a slower transport of these large clasts in the river explain their higher ^{10}Be and ^{26}Al concentrations compared to sand (Fig. 1F).

Finally, by modelling the cosmogenic nuclide acquisition of a population of large clasts (1 mm–30 cm) from their exhumation on the hillslopes to a river outlet, Carretier et al. (2009) investigated how river processes could produce differences in the cosmogenic nuclides in different grain size fractions. In particular, they showed that cobble attrition can yield either a positive or negative relationship according to the river length, cobble attrition rate and initial distribution of the grain sizes on the hillslopes. In practice, this distribution is unknown, and the attrition rate is difficult to quantify as it depends on the lithology, weathering and river dynamics (Attal and Lave, 2006). Carretier and Regard (2011) theoretically investigated the cosmogenic evolution of clasts derived

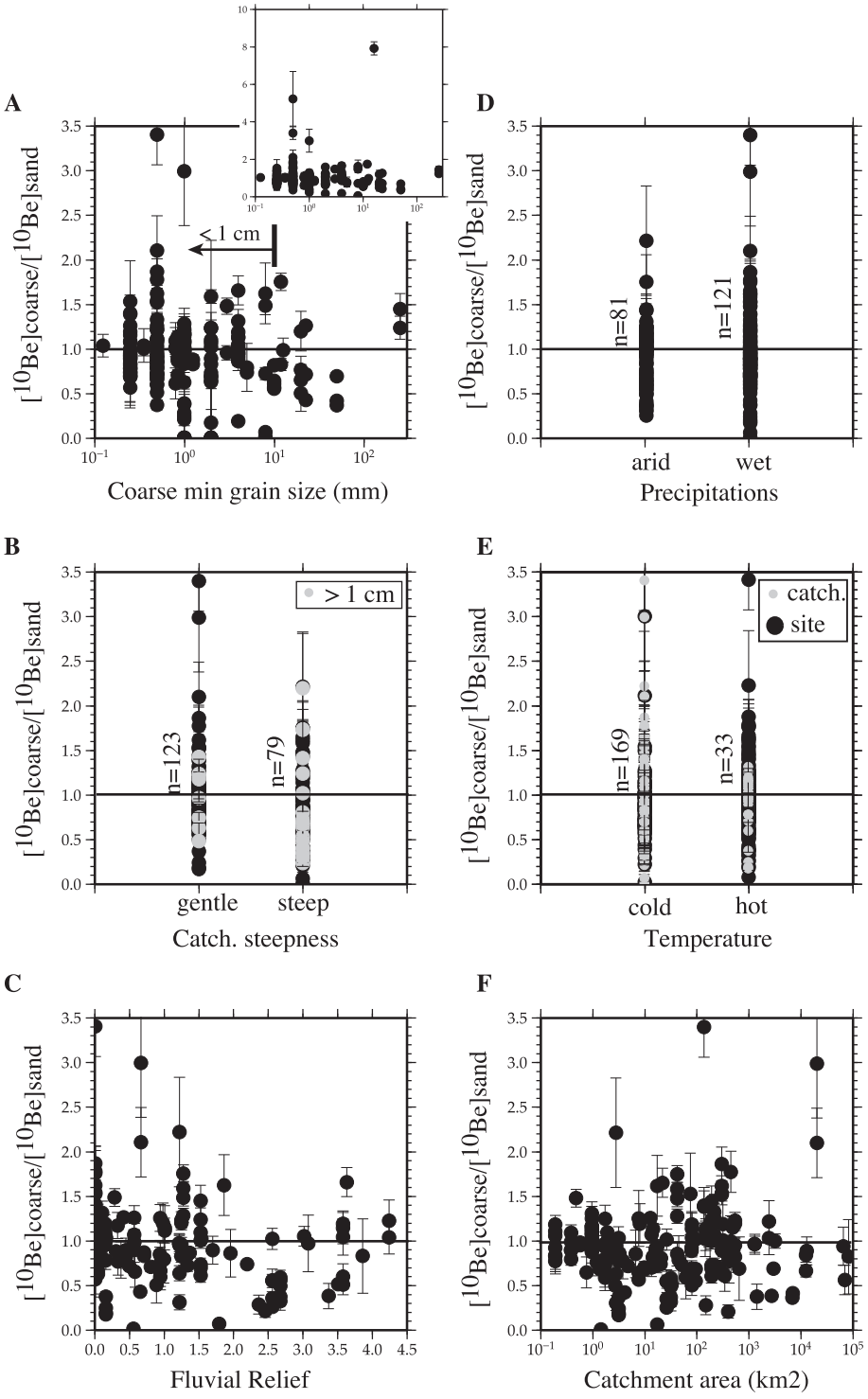

Fig. 2. Data compilation from the literature showing the ratio of ^{10}Be concentration in coarse and fine sediment against different geomorphic and climatic parameters (the original data of this compilation are summarized in Table DR1). Fine sediment is the smallest fraction of a set of samples taken at the same place. Coarse sediment refers to any fraction larger than the fine one. The error bars are calculated by $(y/x)\sqrt{((\sigma x/x)^2+(\sigma y/y)^2)}$ where σ stands for the standard deviation, y for the [^{10}Be] coarse sediment and x for the [^{10}Be] fine sediment. A – Minimum size of the coarse sediment (the maximum size is not always provided). The inset diagram shows the whole set of data. B – Catchment steepness. Based on information given in the papers, we estimated the mean catchment slope. Gentle refers to a mean slope $\leq$ 0.3 m/m and steep to a mean slope >0.3 m/m. The grey points correspond to coarse sediment >1 cm. C – Catchment relief is the difference between the maximum and minimum elevations of the catchment above the sample pair. D – Precipitation. From the provided information and from other sources (cf. comments in Table DR1), we estimated the mean catchment precipitation rate. "Arid" refers to precipitation <0.5 m/yr and "wet" refers to precipitation $\geq$ 0.5 m/yr. E – The same for temperature. The black points correspond to the temperature at the sample location. The grey points are the temperature at the catchment scale, estimated from the catchment relief and a gradient of -6°/km. The catchment hypsometry is not taken into account, thus this temperature is only an estimate of the mean catchment temperature. For both black and red dots, "cold" refers to a temperature $\leq$ 10° C and "hot" refers to temperatures >10° C. F – Catchment areas given in the papers or estimated from maps. This compilation shows no broad relationship between the difference in ^{10}Be concentration between grain sizes and the geomorphic or climatic context, suggesting that the dependence of ^{10}Be concentration on grain sizes deserves another look. (For interpretation of the references to colour in this figure legend, the reader is referred to the web version of this article.)

from a unique source in a catchment, and showed that a weak grain size-transport rate relationship can produce measurable differences in the cosmogenic nuclides between sand, pebbles and cobbles.

Several remarks arise from these studies: 1) there is no general relationship between the difference in the ^{10}Be concentration and grain size. Nevertheless, most studies have analyzed grain size fractions <1 cm (Fig. 2A). Few of them have analyzed the differences between populations of coarser sediment and the studied grain size fractions are different between the studies, which makes a comparison difficult (Aguilar et al., 2014; Belmont et al., 2007; Codilean et al., 2014; Heimsath et al., 2010; Matmon et al., 2003, 2005a; Oskin et al., 2008; Palumbo et al., 2010; Puchol et al., 2014); 2) samples spread out within a catchment show either a clear negative or positive correlation (Aguilar et al., 2014; Brown et al., 1995, 1998; Codilean et al., 2014; Derrieux et al., 2014; Puchol et al., 2014), or variable correlations (e.g. Belmont et al., 2007; Palumbo et al., 2010; Reinhardt et al., 2007; Wittmann et al., 2011b). Variable concentrations are also observed within the same sample divided into different grain size fractions (e.g. Safran et al., 2005); 3) there is no relationship between the difference in the ^{10}Be concentration and catchment area, or the catchment relief (Fig. 2); 4) overall, each difference or absence of difference has an ad-hoc explanation, but the role of certain processes, landslides and size reduction by attrition in particular, seems to be different according to the context; 5) the role of climate, through its capacity to produce soil and to transport grain sizes at different or similar rates in the river has been mentioned (e.g. Clapp et al., 2001), but remains largely unexplored.

3. Regional context and methods

3.1. Previous related studies in this region

Although this paper is not focused on the erosion rates, it is useful to recall previous studies that have used cosmogenic nuclides to quantify erosion rates in or near the study region. On the western side of the Andes in Perú and Chile, previous studies have quantified catchment-scale erosion rates (Abbuehl et al., 2011a,b; Aguilar et al., 2014; Carretier et al., 2013, 2014; Jungers et al., 2013; Kober et al., 2009; McPhillips et al., 2013). The values range between 10^{-4} and 1 mm/yr. In northern Chile, Kober et al. (2009) observed larger (but with overlapping error bars) ^{10}Be, ^{26}Al and ^{21}Ne concentrations in the 1–2 mm fractions compared to the smaller fractions in two samples. In central Chile, Aguilar et al. (2014) obtained smaller ^{10}Be concentrations in pebbles (5–10 cm) compared to sand. Ages for marine terraces, river terraces, alluvial fans and landslides were also obtained in Perú and Chile (Antinao and Gosse, 2009; Dunai et al., 2005; Evenstar et al., 2009; Hall et al., 2008; Jungers et al., 2013; Kober et al., 2007; Nishiizumi et al., 2005; Quezada et al., 2007; Melnick et al., 2009; Rodríguez et al., 2013; Saillard et al., 2009, 2011), showing erosion rates for these markers that are smaller than 10^{-3} mm/yr in desertic areas, which were used to obtain surface ages as old as the Mio-Pliocene (Dunai et al., 2005; Kober et al., 2007; Nishiizumi et al., 2005). On the other side of the range, catchment scale erosion rates were obtained in Ecuador (Vanacker et al., 2007a,b), the Amazon basin (Wittmann and VonBlanckenburg, 2009; Wittmann et al., 2009, 2011b,c,a), Bolivia (Hippe et al., 2012; Safran et al., 2005) and Argentina (Baker et al., 2009; Pepin et al., 2013; Walcek and Hoke, 2012), with a similar range of values as in the western side of the Andes.

The studied catchments are topographically transient, responding to a surface uplift that occurred in the Miocene, and which is evidenced by perched relicts of low relief surfaces and knick-points in the main rivers (e.g. Aguilar et al., 2011; Bissig et al., 2002; Rehak et al., 2010; Schildgen et al., 2007; Steffen et al., 2009; Thouret et al., 2007; Trauerstein et al., 2013). This ongoing adjustment of the topography is characterized by strong differences in the slope within the catchments between areas that have experienced this adjustment and the rest of the catchment. This situation results in probable heterogeneous erosion rates within the catchments (e.g. Kober et al., 2009; Walcek and Hoke, 2012) which may have an effect on the difference in the ^{10}Be concentration between sand and coarser sediment, as discussed below.

3.2. Sampling

The sampled catchments are situated along the western margin of the Perúvian and Chilean Andes (Fig. 3). A wide range of climatic contexts is investigated in this study, from arid in the north (precipitations <10 cm/yr), to humid south of 35°S (>2 m/yr) (Fig. 4). It was assumed that this gradient results in different erosion rates and thus different values for the ^{10}Be concentrations, which are useful for the present analysis. In particular, the erosion rates in Chile between 27 and 35°S show a sharp peak near 32° at the transition between arid and wet climates (Pepin et al., 2010; Carretier et al., 2013).

We adopted a regional sampling strategy, collecting sediment in a similar tectonic and geomorphic position, at the outlet of the major rivers ([1200–7300] km^2) draining the main Cordillera (Fig. 3).

At each point, we sampled ~2 kg of sand at different places within a perimeter of several tens of meters from the river bank. In the same area, we collected (1) between 50 and 100 pieces of gravel with median sizes in the [1–3] cm range and (2) between 6 and 30 rounded pebbles in the [5–10] cm range (Fig. 4A). These sizes correspond to the median dimension (b axis) of the ellipsoids. The maximum dimension (c axis) can reach 5 cm in the case of the gravel and 12 cm in the case of the pebbles. We crushed and mixed all of the gravel at the GET laboratory (Toulouse). The three pebbles samples that contain 6 or 15 clasts were collected at the beginning of the sampling campaign. We crushed the whole pebbles at the GET laboratory and mixed them together. For the other samples, we cut, in the field, a piece representing approximately one third of each pebble. Then we crushed these pieces in the lab and mixed them together. The expected relative difference in the mean ^{10}Be concentration between a piece of each pebble of that size and the concentration in the whole pebble should not exceed several percent (Carretier and Regard, 2011). This procedure allowed us to carry more pebbles with us out of the field, and thus to improve the estimation of the average ^{10}Be concentration in the pebble population. The [0.5–1] mm fraction of the crushed material was analyzed in all three cases (sand, gravel and pebbles).

The Andean catchments are characterized by a large variety of underlying lithologies, with a variable proportion of granitoid intrusives (Fig. 5). No lithological distinction can be made for sand grains, meaning that they can come from any place in the catchment where the substratum contains quartz. On the contrary, we restricted the lithology of the pebbles and gravel to granitoid rocks. These rocks are mainly granodiorites and granites that are Mezozoic and Cenozoic in age (Fig. 4A), for which the sources in the studied catchments are mapped (e.g. Charrier et al., 2007, or the 1/1,000,000 Geological maps of Chile and Perú). No pure quartz pebbles were sampled, to avoid samples coming from quartz dykes which could erode differently compared to granitoid. We acknowledge that limiting the sampling of the gravel and pebbles to a particular rock found within a catchment may complicate the comparison with sand, which can derive from all quartz-rich rocks.

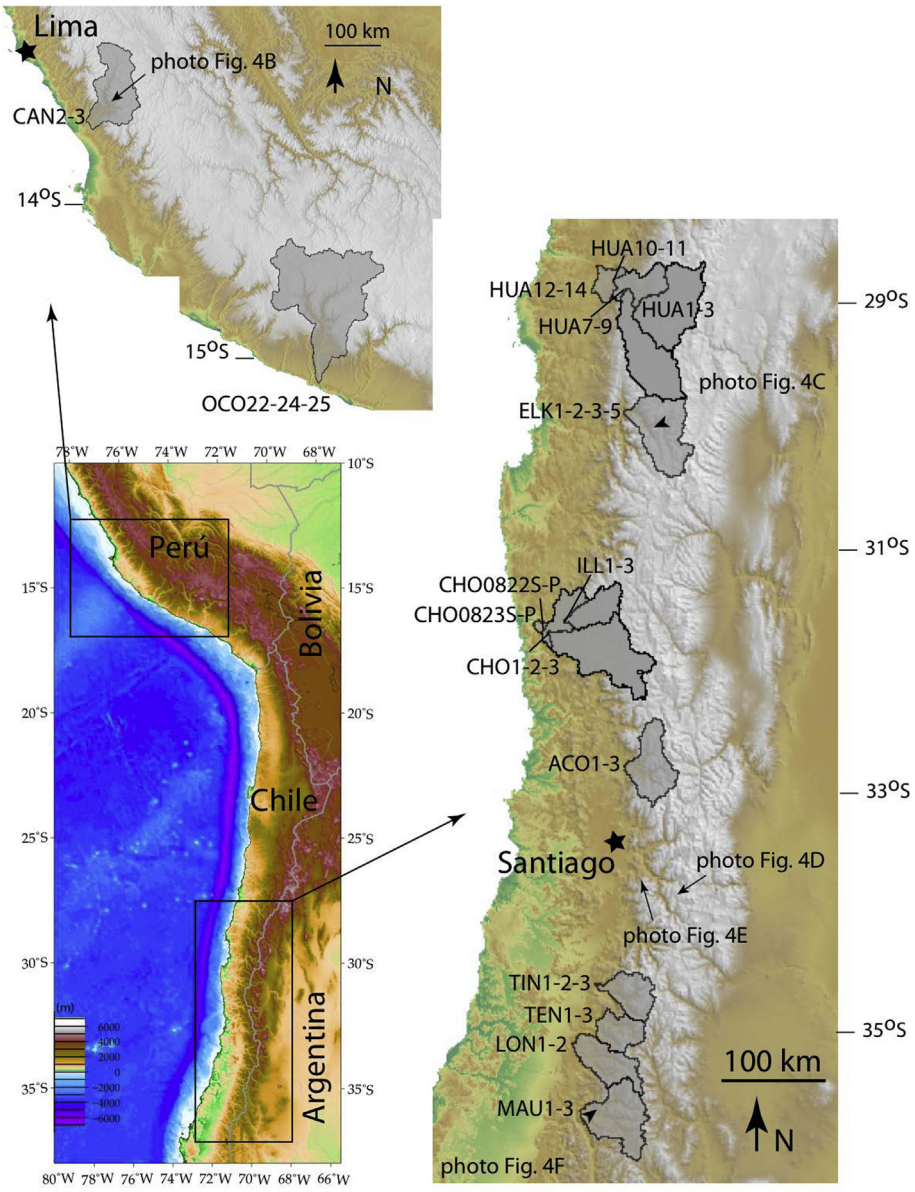

Fig. 3. Maps showing the location of the studied catchments above the samples identified by their code in Tables 1 and 2.

On the other hand, sampling a representative fraction of all rocks is practically impossible. This would require knowing a priori the contribution of each lithological patch to the total coarse sediment flux and the attrition rate for each lithology (e.g. Attal and Lave, 2006). Instead, we preferred to select granitoid clasts as we were able to identify their source in each catchment. In the results section, we analyze the possible differences between the mean ^{10}Be production rate of granitoids and that of the whole area of each catchment.

In addition, we estimated the grain size distribution of the river bed surface layer (~30 cm) at several sampling points by measuring the relative weight of four sediment size fractions ([0–1.2] cm, [1.2–3.6] cm, [3.6–10] cm, >10 cm). The total weight of the collected sediment (50–70 kg) is probably too small to represent an accurate distribution of the clast size (Attal and Lave, 2006), but it provides an estimate of the D_{50} that we hypothesized as being useful to describe the differences in the sediment mixtures between the studied sites (Table 1).

3.3. ^{10}Be concentration and production rates

Samples were prepared following the protocol described in von Blanckenburg et al. (1996). Some of the samples were prepared in the GET laboratory and the others in the LN2C facility in Cerege (Aix en Provence) (see Table 2). The ^{10}Be/^{9}Be Be ratio was obtained at the LN2C ASTER AMS and calibrated directly against the National Institute of Standards and Technology standard reference material 4325 by using an assigned value of (2.79 ± 0.03).10E-11 (Nishiizumi et al., 2007).

In order to analyze if the differences in the ^{10}Be concentration in sand versus coarser sediment are related to differences in the provenance (zones dominated by landslides or zones with granitoids), we calculated the different mean ^{10}Be production rates for each catchment: (1) a catchment-mean ^{10}Be production rate for the whole catchment area underlined by quartz-rich rocks, (2) a granitoid-mean ^{10}Be production rate for granitoid only, and (3) a steep granitoid-mean ^{10}Be production rate for granitoid with slopes

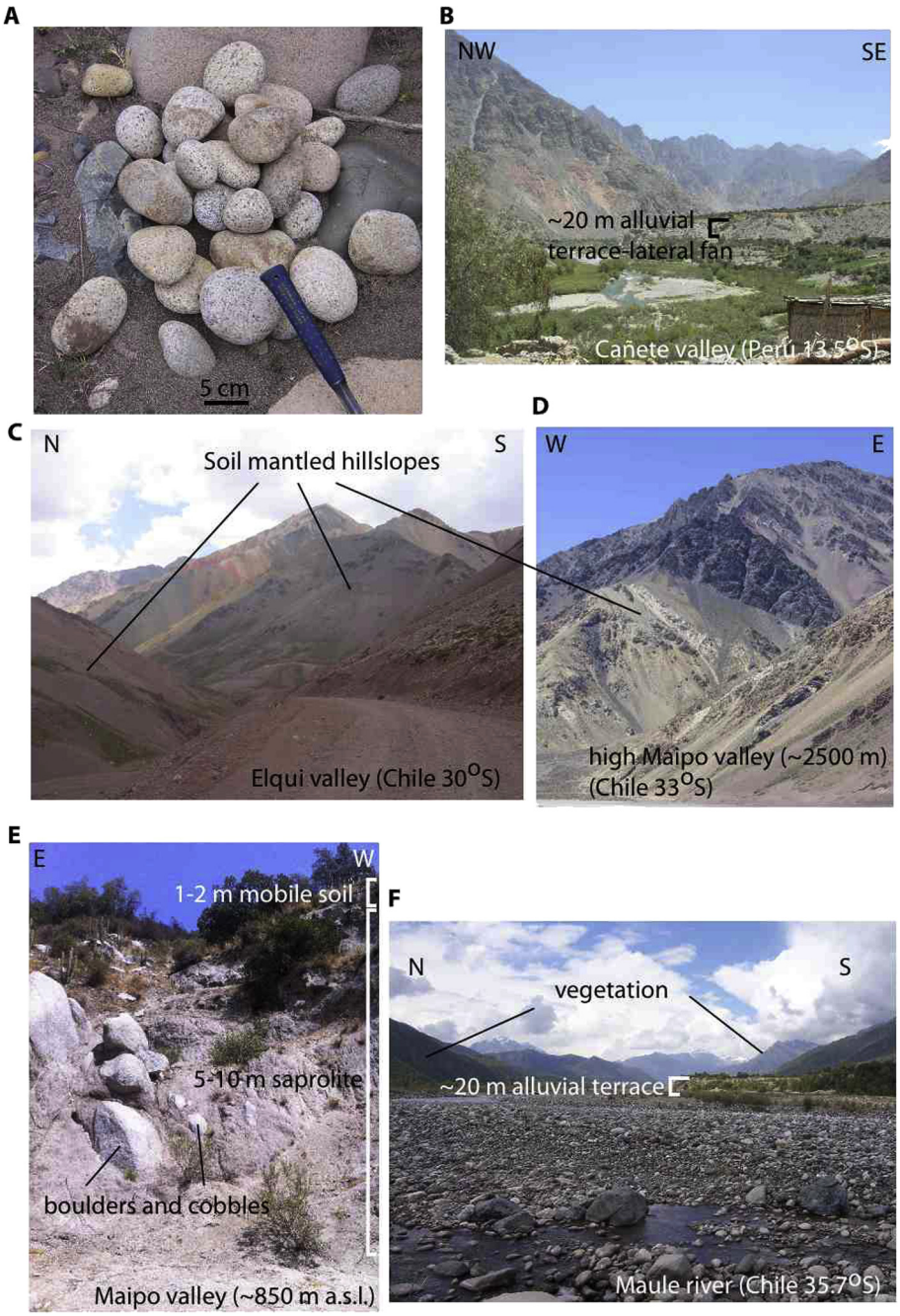

Fig. 4. A – Example of selected pebbles in the range of [5–10] cm (median size or b-axis of the ellipsoid equivalent) showing the granitoid lithology. B – Example of an alluvial terrace and lateral fan incised by the river in the Cañete valley, Perú. C and D – Example of soil-mantled hillslopes in two catchments in the semi-arid zone. E – Soil-mantled and thick saprolite affecting granitoid in the Maipo valley region of Santiago, Chile. F – Example of a river cutting into an alluvial terrace in the Maule valley. See locations on Fig. 3.

greater than 0.6 (~tan 30°), assuming that such slopes are prone to mass wasting.

The SRTM 90 m digital elevation model was used to determine the elevations. The catchment-mean ^{10}Be production rate was calculated by the following procedure (Table 1) (see Carretier et al., 2013, 2014, for the Chilean catchments):

1 The surface ^{10}Be production rate was calculated for each catchment pixel using the Stone (2000) production model and a sea level high elevation production rate of 4.5 at g^{-1} (Balco et al., 2008).
2 The production rate for each pixel was multiplied by an estimate of the topographic shielding factor, ranging between 0 and 1, using the method provided by Codilean (2006). The topographic shielding factor varies between 0.85 and 1 and averages close to 0.99 for all of the studied catchments.
3 The ^{10}Be production rate for each pixel was multiplied by the relative proportion of quartz in the underlying lithology in order to limit the bias due to lithological variations (Safran et al., 2005). This relative proportion is given by $\chi_i/\sum_1^n \chi_i$ where χ_i is the percentage of quartz in the lithology of pixel i and n is the number of pixels of the considered catchment (Safran et al., 2005). The catchment lithologies were obtained from the 1/1000000 Geological Maps of Chile and Perú. For each lithology, we estimated the proportion of quartz minerals from the

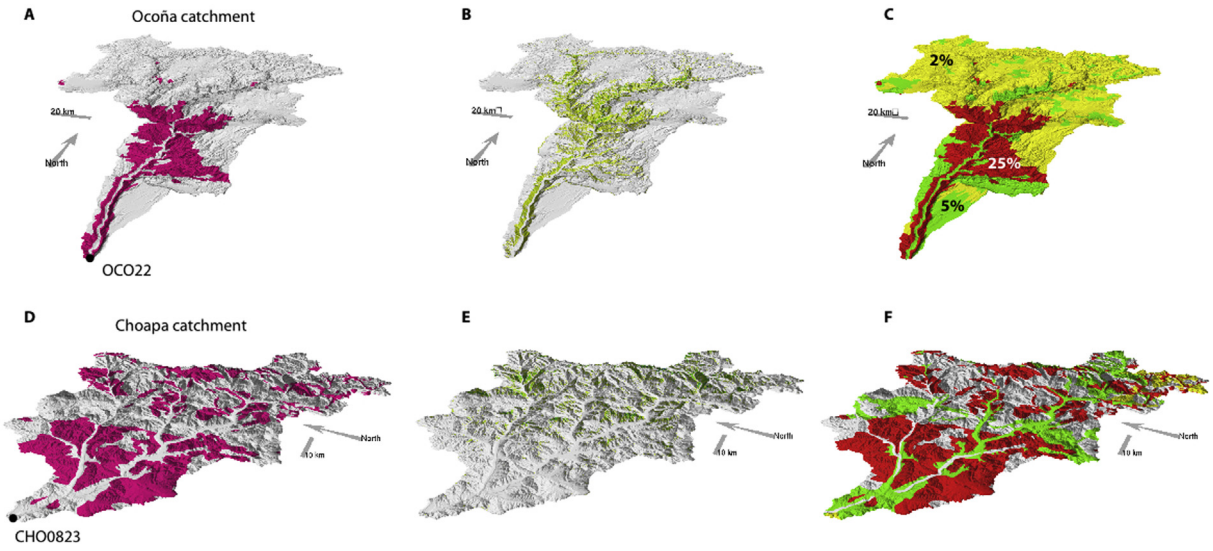

Fig. 5. A to F: Examples of masks used to calculate the ^{10}Be production rates for specific zones, trying to explain the differences in the ^{10}Be concentrations in terms of the different provenances for coarse and fine sediments. These two catchments are displayed as illustrative examples: A-B-C: Ocoña in Perú. D-E-F: Choapa in Chile (see location in Fig. 3). A and D: Granitoids in pink. B and E: Slope greater than 0.6 m/m in green. C and F: Proportion of Quartz for the different lithologies (indicated by numbers in C) based on the 1/1000000 geological maps of Perú and Chile. (For interpretation of the references to colour in this figure legend, the reader is referred to the web version of this article.)

description of the lithological maps and from microscopic observations of samples collected from the high Andes between 33°30′S and 35°S (Reynaldo Charrier, personal communication, 2010). The estimated proportions of quartz are: Granitoid rocks: 25%, Rhyolitic volcanic rocks: 5%, Undifferentiated detritic rocks: 5%, Ignimbrites: 2%, Other lithologies: 0%.

4 These corrected surface ^{10}Be production rates were averaged at the catchment scale.

The granitoid-mean ^{10}Be production rate and the steep granitoid-mean ^{10}Be production rate were obtained following steps 1, 2 and 4, by selecting granitoid pixels and granitoid pixels with slopes larger than 0.6, respectively (Table 1).

The estimate of the quartz content in each lithology has an uncertainty. In order to estimate the effect of this unknown uncertainty on the ^{10}Be production rates, we also calculated the uncorrected catchment-mean ^{10}Be production rates, without correcting for the quartz content (see Carretier et al., 2014, for the Chilean catchments). These corrected production rates are, on average, 15% larger than the uncorrected rates (between 2% smaller for TEN1 and 54% larger for OCO22 – Table 1), and smaller than the spatial variations of the ^{10}Be production rates. These differences depend mainly on the hypsometry of granitoids in each catchment.

3.4. Catchment erosion rates

We quantified the millennial catchment mean erosion rates using the ^{10}Be concentration in sand. We assumed that this concentration corresponds to a secular equilibrium between the loss by erosion and the gain by production on the hillslopes and we did not take the radioactive decay of ^{10}Be (Brown et al., 1995; Granger et al., 1996; von Blanckenburg, 2005) into account. We calculated the mean catchment erosion rates ε [L/T] corresponding to the sand ^{10}Be concentration [^{10}Be] using the following equation:

$$\varepsilon = \frac{\wedge_n f_n P}{\rho[^{10}Be]} + \frac{\wedge_{\mu s} f_{\mu s} P}{\rho[^{10}Be]} + \frac{\wedge_{\mu f} f_{\mu f} P}{\rho[^{10}Be]} \quad (1)$$

where P is the catchment-mean production rate (corrected for the lithology), $\rho = 2700$ kg/m^3, $\wedge_n = 160$ g/cm^2, $\wedge_{\mu s} = 1500$ g/cm^2 and $\wedge_{\mu f} = 5300$ g/cm^2 are effective apparent attenuation lengths for the neutrons, negative muons, and fast muons, respectively, and $f_n = 0.9785$, $f_{\mu s} = 0.015$ and $f_{\mu f} = 0.0065$ are the relative contributions of the three reactions to the total ^{10}Be production (Braucher et al., 2003). Using the new muon contribution estimate of Braucher et al. (2013) (with an attenuation length of 4300 g/cm^2 for muons without distinguishing between negative and fast muons), the erosion rates are 0.6% smaller. For the Chilean catchments, the erosion rates given here are those from Carretier et al. (2014), calculated following the procedure cited above, and recalculated from Carretier et al. (2013) by including fast muons. These recalculated erosion rates are ~10% lower than the initial values provided by Carretier et al. (2013).

3.5. Geomorphic and climatic parameters

The catchment delimitation, mean slope and area were calculated using the SRTM 90 m digital elevation model. The catchment mean slope is calculated using a 3 × 3 pixel averaging procedure (r.slopeaspect of function in GRASS).

We estimated the normalized catchment-mean channel steepness k_{sn} for each catchment. This index is calculated following a procedure similar to the one proposed by Wobus et al. (2006). This procedure is automatic. The drainage network is extracted assuming a critical drainage area of 8.1 km^2 (a large value to avoid glacial valleys). The drainage is divided into segments of different sizes (output of the r.watershed function in GRASS). For each segment, the elevations are smoothed out using a 2 km wide moving Gaussian window, the local slopes S are calculated from the smoothed profile and are fitted by the function $S = k_{sn}A^{0.5}$ from which k_{sn} is calculated (A is the drainage area in m^2). A drainage-mean k_{sn} is calculated by averaging the values of the drainage segments and weighting by their length. We also estimated the mean k_{sn} by simply dividing the steepest-descent slope by the root square of the drainage area for the drainage pixels and then averaging it. Both values fit within a 10% difference in average. The values for the Chilean catchments are from the Data Repository of Carretier et al. (2013).

We compare the ^{10}Be concentrations to the catchment-mean temperature and to the runoff. The runoff value is taken from

Table 2
Data used in Figs. 4 and 5. The erosion rates are calculated from the $^{10}Be_{sand}$ and catch.-mean ^{10}Be production rate (corrected for Qz). Their uncertainty is 1σ and they incorporate a 15% external uncertainty on the ^{10}Be production rate. Except for CAN2 and OCO22, the erosion rates are from Carretier et al. (2014), who recalculated the values initially calculated by Carretier et al. (2013) by taking fast muons into account (which results in erosion rates that are ~ 10% lower in average compared to Carretier et al. (2013)). The runoff in Chile is from Pepin et al. (2010). Catchment mean temperatures in Chile are from Carretier et al. (2013). The runoff in Perú is from Lavado et al. (2012).

Catchment	$^{10}Be_{sand}$ (atoms/g) [0.5–1] mm	$^{10}Be_{gravels}$ (atoms/g) [1–3] cm	$^{10}Be_{pebbles}$ (atoms/g) [5–10] cm	catch.-mean ^{10}Be prod. rate (corrected for Qz) (at/g/yr)	Granitoid-mean ^{10}Be prod. rate (at/g/yr)	Steep granitoid-mean ^{10}Be prod. rate (Slope > 0.6) (at/g/yr)	Uncorr. catch.-mean ^{10}Be prod. rate (at/g/yr)	Area (km)2	Area granitoids (km^2)	3 × 3 slope (m/m)	Median bedload size (cm)	Catch mean Temp. (Co)	Runoff (m/yr)	Erosion rate (mm/yr)
CAN2	3.28E+05 ± 2.1E+04	–	5.27E+04 ± 7.8E+03	28.4	24.1	19.3	36.1	5794	1336	0.44	98	4.4	2.6E-01	5.1E-02 ± 8E-03
OCO22	9.95E+04 ± 1.3E+04	3.23E+04 ± 2.2E+03	7.35E+03 ± 1.2E+03	24.8	14.6	14.5	38.2	15826	1997	0.29	50	3.2	1.3E-01	1.5E-01 ± 3E-02
HUA1	4.80E+05 ± 1.4E+04	–	3.32E+05 ± 1.8E+04	41.0	40.7	36.1	43.9	3176	1886	0.44	28	4.0	3.5E-02	5.0E-02 ± 8E-03
HUA12	5.99E+05 ± 2.5E+04	–	2.49E+05 ± 1.2E+04	37.4	38.2	35.3	37.7	7834	3735	0.42	–	2.6	3.5E-02	3.7E-02 ± 6E-03
HUA10	5.89E+05 ± 1.7E+04	–	2.16E+05 ± 1.9E+04	39.0	39.5	35.3	40.0	7245	3567	0.43	–	5.0	3.5E-02	3.9E-02 ± 6.E−03
HUA7	8.33E+05 ± 5.4E+04	3.19E+05 ± 2.7E+04	–	41.5	42.4	36.8	42.6	2914	1193	0.45	59	4.6	3.5E-02	2.9E-02 ± 5E-03
ELK1	1.77E+05 ± 2.3E+04	3.71E+05 ± 3.0E+04	1.38E+05 ± 1.2E+04	38.6	38.3	30.5	45.8	2921	1172	0.47	36	4.8	6.9E-02	1.2E-01 ± 2E-02
ILL2	4.69E+05 ± 1.4E+04	7.68E+05 ± 6.4E+04	–	22.9	23.7	23.5	24.7	1231	360	0.4	–	7.2	7.6E-02	2.9E-02 ± 4E-03
CHO0823	2.18E+05 ± 9.5E+03	–	2.34E+05 ± 7.8E+03	17.0	16.9	22.6	20.2	5998	2129	0.36	–	8.7	7.6E-02	4.6E-02 ± 7E-03
CHO0822	1.98E+05 ± 5.8E+03	–	9.85E+04 ± 5.8E+03	17.2	16.9	22.6	20.4	5903	2119	0.36	61	8.6	7.6E-02	4.5E-02 ± 7E-03
CHO1	1.96E+05 ± 6.7E+03	4.21E+05 ± 3.80E+04	7.95E+04 ± 3.2E+03	18.9	18.5	23.0	21.9	3757	1310	0.37	–	7.7	6.6E-02	5.7E-02 ± 9E-03
ACO1	1.01E+05 ± 2.9E+03	1.94E+05 ± 1.9E+04	–	33.0	33.6	30.2	37.0	2123	218	0.51	–	5.8	5.1E-01	1.9E-01 ± 3E-02
TIN1	9.94E+04 ± 5.3E+03	1.77E+05 ± 1.7E+04	7.39E+04 ± 1.35E+04	26.3	27.1	30.6	27.5	1465	240	0.48	50	4.0	1.2E+00	1.6E-01 ± 2.5E-02
TEN1	7.33E+04 ± 4.81E+04	–	1.06E+04 ±.4E+03	20.4	19.1	18.2	19.9	1225	66	0.47	–	5.8	1.6E+00	1.6E-01 ± 1.1E-01
LON1	6.44E+04 ± 2.91E+04	4.66E+04 ± 1.17E+04	–	12.5	8.6	12.6	17.3	1789	77	0.34	–	6.8	1.9E+00	1.1E-01 ± 5.5E-02
MAU1	1.29E+05 ± 1.5E+04	–	1.26E+04 ± 2.5E+03	18.9	18.8	17.7	21.8	2693	508	0.37	–	6.6	1.9E+00	8.6E-02 ± 1.6E-02

Pepin et al. (2010) and corresponds to the annual average daily water discharge measurements at the Dirección General de Aguas (DGA-Ministerior de Obras Públicas, Chile) gauging stations, divided by the catchment area (the resulting dimension in is m/a) (see details in Pepin et al., 2010). We selected the closest gauging station to each sand sample location (at the same place up to ~50 km apart). The data are from "DGA. 1987. Balance Hidrico de Chile". p. 23. They correspond to the mean annual averages at fixed meteorological stations over periods of time ranging between 3 and 30 years. The studied catchments have different hypsometries, so that the mean temperature at the catchment outlet does not give a meaningful estimate of the temperature differences between the catchments. For each catchment, the catchment-mean temperature is estimated by assuming a temperature-elevation gradient of $-4.5\ ^{\circ}C\ km^{-1}$. This gradient is lower than the often used value of $-6\ ^{\circ}C\ km^{-1}$, but it is the maximum estimated from the only temperatures available ($n = 10$) at the different elevations within three mountainous catchments of central Chile. The resulting catchment-mean temperatures range between 2 and 8 °C.

4. Results

4.1. ^{10}Be concentrations

Table 1 shows that the ^{10}Be e concentration in sand varies geographically over two orders of magnitude in the range $[10^4–10^6]$ at/g. These differences are explained by differences in the catchment erosion rates and by the differences in the catchment elevations: the ^{10}Be concentrations are high in the arid and elevated north, and low in the wet and lower mountains of central Chile, as shown by Carretier et al. (2013). Repeated sampling of sand at the same location in the Elqui River (ELK1 and ELK2) gave identical ^{10}Be concentrations within 1σ (Table 2).

Fig. 6A shows the latitudinal variations of the ^{10}Be concentration ratio between coarse sediment (gravel and pebbles) and sand. Eleven pebble samples have lower ^{10}Be concentrations (ratio between 0.1 and 0.8) than sand, while one sample pair (CHO0823S-CHO0823G) has overlapping ^{10}Be concentrations within 1σ. The gravel samples have lower ^{10}Be concentrations than sand in three cases (a ratio between 0.35 and 0.75), and higher concentrations (a ratio between 1.5 and 2.3) in five other cases. In the Perúvian Ocoña River, gravel (OCO25) and pebbles (OCO24) both contain lower ^{10}Be concentrations than sand, whereas in three other cases (ELK1, CHO1 and TIN1), gravel and pebbles show an inverse relationship.

4.2. Possible bias associated with the granitoid hypsometry

The studied catchments show variable distributions of granitoid rocks (e.g. Charrier et al., 2007), which contain a higher proportion of quartz, and which are the source of the sampled gravel and pebbles (Fig. 5). If the granitoid rocks are mainly concentrated at low elevations (a lower ^{10}Be production rate), this may explain the lower ^{10}Be concentration in the gravel and pebbles, and vice versa. Fig. 7A shows a comparison between the ^{10}Be concentration ratios for the coarse and sand fractions and the ratios for the granitoid and catchment ^{10}Be production rates. Both ratios should fit along the 1:1 line if the hypsometry of the granitoid rocks was responsible for the observed differences in the ^{10}Be concentration (assuming that they erode at the same rate as the other lithologies). Actually, the granitoid ^{10}Be production rate is less than 5% lower than the catchment-mean ^{10}Be production rate, except for catchments OCO22 and CAN2 (Perú), and LON1 (Chile) (Fig. 7A). For the pebble samples from OCO22-24 and the gravel samples from OCO22-25 (Ocoña catchment in Perú), the low elevation of the granitoid does not explain by itself their lower ^{10}Be concentrations as their

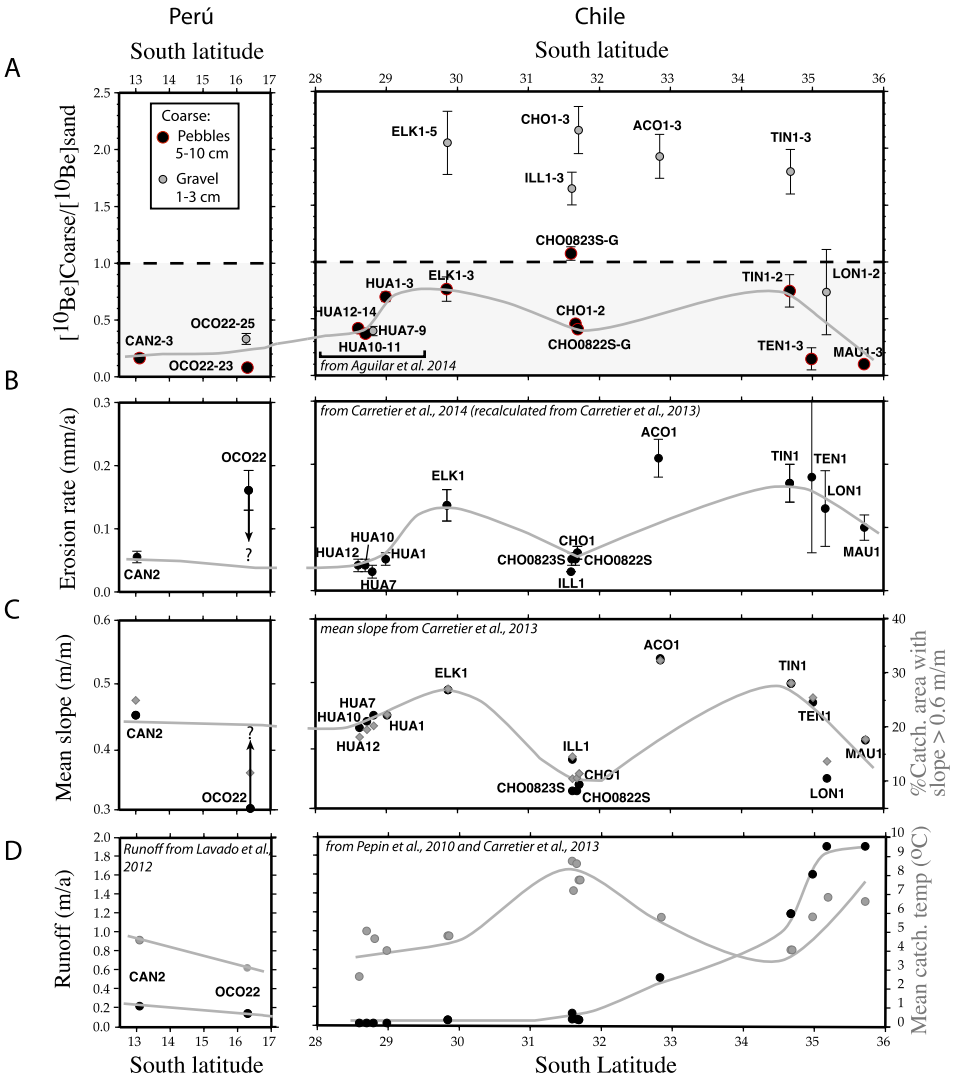

Fig. 6. A – Latitudinal variations of the ^{10}Be concentration ratio for coarse sediment and sand. B – Catchment-mean erosion rate. C – Catchment-mean slope. D – and catchment-mean annual temperature and runoff. The grey lines underline the possible co-variations in the catchment-mean slope, proportion of steep slopes >0.6 m/m, erosion rate and ^{10}Be concentration ratio when this ratio is <1. The sand fraction is [0.5–1] mm.

points lie below the 1:1 line. Conversely, the low elevations of the granitoid exposure explains the lower ^{10}Be concentrations for the gravel samples from LON1 (the Lontué catchment in Chile) compared to that of sand (Fig. 7A). In order to test if the result depends on our estimations of quartz content, we also analyzed the relationship between these ratios using the uncorrected catchment-mean ^{10}Be production rate in Fig. 7B. The resulting range in the ratio between the granitoid and catchment ^{10}Be production rates is higher. The points OCO22-25 and ELK1-3 are now close to the 1:1 line, but the previous conclusion is still valid for the other points. To sum up, except for gravel samples LON1-2 and possibly OCO22-25 and ELK1-3, the hypsometry of the granitoids (i.e. the provenance of the gravel and pebbles) does not explain the observed differences in the ^{10}Be concentration between the coarse and sand fractions.

Fig. 7C illustrates a possible influence of the proportion of the catchment area underlain by granitoid on the ^{10}Be concentration ratio between pebbles and sand. This weak trend suggests that when there are low amounts of granitoid in a catchment, the mean ^{10}Be concentration in pebbles is lower than that of sand. No correlation is observed for gravel.

In order to study if gravel and pebbles could come preferentially from the steep granitoid areas prone to landslides and high erosion rates, as suggested by previous studies in this area (Aguilar et al., 2014) and elsewhere (Belmont et al., 2007), we plotted the ^{10}Be concentration ratios between the coarse and sand fractions against the ratio for the steep granitoid and catchment ^{10}Be production rates in Fig. 7D. The steep granitoid ^{10}Be production rate is defined as the mean ^{10}Be production rate for the granitoid areas with slopes greater than 0.6 m/m (~tan30°), and for which mass wasting and high erosion rates may dominate (e.g. Roering et al., 1999; Binnie et al., 2007; Carretier et al., 2013). For pebbles and gravel with a lower ^{10}Be concentration than sand, there may be a weak positive relationship between both ratios. This would suggest a combination of two processes: 1 – pebbles and gravel with low concentrations are preferentially sourced from steep granitoid areas, and 2 – these areas have a higher erosion rate, explaining the lower ^{10}Be concentration, as suggested by Aguilar et al. (2014) for the Huasco catchment. When the contribution of steep granitoid to the mean ^{10}Be production rate increases, the proportion of sand sourced from high erosion rate areas also increases, so that the difference between pebbles and sand decreases (the ratio tends towards 1 in Fig. 7D).

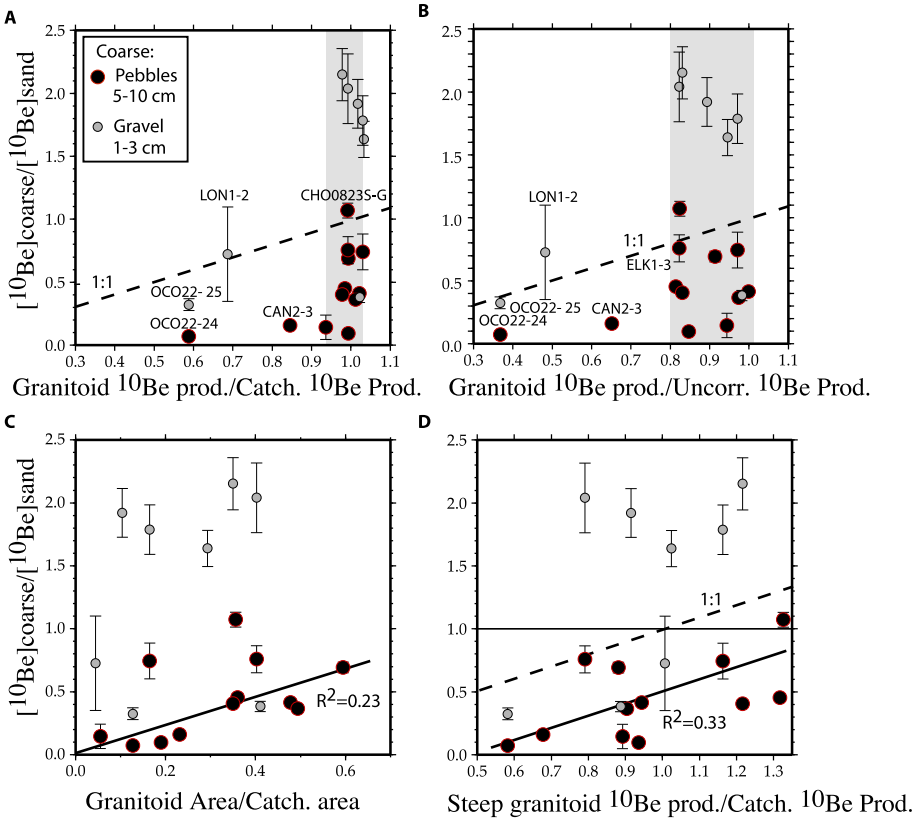

Fig. 7. Relationships between the ^{10}Be concentrations in coarse and sand sediment ([^{10}Be e]coarse/[^{10}Be]sand) and parameters concerning granitoid rocks: A-granitoid ^{10}Be production rate ratio (calculated for granitoid only) and catchment-mean ^{10}Be production rate. B – Same as A – but using the catchment-mean ^{10}Be production rate uncorrected for the lithology. C – Granitoid area/catchment area ratio. D – Same as A – but selecting slopes >0.6 m/m to calculate the steep granitoid ^{10}Be production rate. The sand fraction is [0.5–1] mm.

4.3. Relationship with the erosion rate

Differences in the catchment-mean erosion rate may be associated with different contributions of mass wasting to hillslope denudation, different storage times in the drainage network, or different attrition rates for the cobbles. As these processes have been proposed to explain the differences in the ^{10}Be concentration between coarse and fine river sediment, we explored the relationship between the catchment-mean erosion rate and the [^{10}Be]gravel/[^{10}Be]sand and [^{10}Be]pebble/[^{10}Be]sand ratios.

Fig. 6 shows the latitudinal pattern of these values. There is no clear relationship over the entire dataset. If we exclude the samples with a higher ^{10}Be concentration in pebbles or gravel than in sand, there is some latitudinal correlation between the erosion rate and the [^{10}Be]coarse/[^{10}Be]sand ratio, symbolized by the grey line in Fig. 6A and B. Higher erosion rates seem to be associated with a smaller difference between the ^{10}Be concentration in coarse sediment and sand. OCO22 in Perú deviates from this trend, but the erosion rate estimated for this catchment strongly depends on the choice for the contributing area to erosion: assuming that most of the river sediment comes from actively eroding areas, which excludes the Altiplano part of this catchment, the calculated erosion rate would be divided by ~ 2, and would thus correspond to the latitudinal trend (the mean slope would also increase – Fig. 6C). A lower [^{10}Be]coarse/[^{10}Be]sand ratio associated with a higher erosion rate may be consistent with a higher contribution of mass wasting to hillslope erosion: when this contribution increases, the proportion of sand derived from the landslides also increases, so that the sand and pebbles have similar sources. Nevertheless, no relationship appears when plotting the erosion rate against the [^{10}Be]coarse/[^{10}Be]sand ratio (Fig. 8).

4.4. Relationship with the topography

We explored the correlations between the [^{10}Be]gravel/[^{10}Be]sand ratios and several geomorphic parameters, as illustrated by Figs. 6 and 9. There is no relationship between these ratios and the catchment area, except for gravel with a higher ^{10}Be concentration than sand. For these samples, the excess in the ^{10}Be concentration in gravel increases with the size of the catchment area (Fig. 9A). No correlation is seen with the catchment-mean elevation (Fig. 9B) for the ratios <1. However there is a positive correlation for the gravel with a ratio >1, excluding CHO1, which has the larger catchment area (Fig. 9A). The D_{50} of the sediment mixture in the river does not seem to affect the [^{10}Be]gravel/[^{10}Be]sand ratio, where data exist (Fig. 9C).

No clear relationship appears on the graphs plotting the [^{10}Be]coarse/[^{10}Be]sand ratios against the granitoid slope (Fig. 9D), or the catchment-mean slope (Fig. 9E). The [^{10}Be]coarse/[^{10}Be]sand ratio also does not fit with the normalized steepness index k_{sn} for the drainage network (Fig. 9F).

Latitudinally, some covariation appears between the slope, erosion rate (see Carretier et al., 2013, 2014, for details about the effect of slope on the erosion rate in Chile), and [^{10}Be]coarse/[^{10}Be]sand ratio when this ratio is <1 (Fig. 6C). This makes sense if steeper slopes and larger erosion rates are associated with a larger proportion of the catchment area with high erosion rates and mass wasting, as discussed above. This suggests that the grain size dependence of the ^{10}Be concentration may depend on the transient

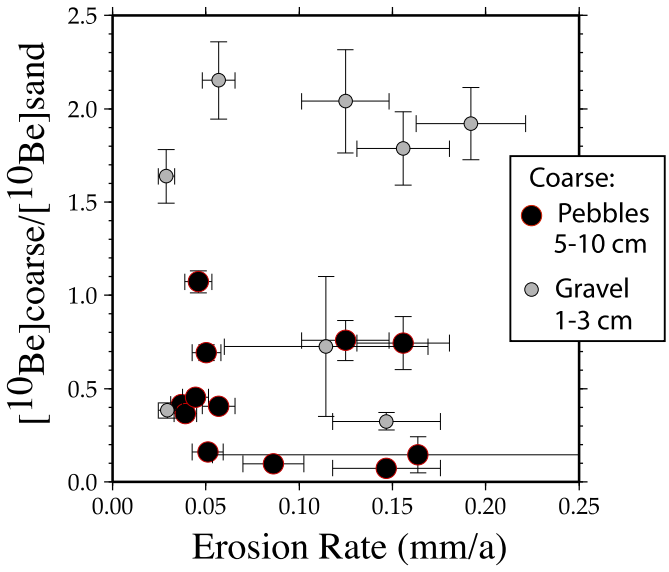

Fig. 8. Relationships between the ^{10}Be concentrations in coarse and sand sediment ([^{10}Be]coarse/[^{10}Be]sand) and catchment-mean erosion rates. The erosion rates are calculated from the ^{10}Be concentrations in sand and using the catchment-mean ^{10}Be production rate corrected for the lithology (Table 2). The sand fraction is [0.5–1] mm.

stage of the catchments. Catchments that have a large proportion of area that is unaffected by the ongoing steepening associated with the Miocene uplift may exhibit a large difference between the ^{10}Be concentration for different grain sizes. In order to test this, we plotted the proportion of the catchment area with slopes >0.6 in Fig. 6C. The catchments with a low proportion are those with a large proportion of relict topography unaffected by the ongoing incision (for instance, the Ocoña catchment in Perú – Fig. 5). There is no clear relationship between the proportion of steep areas and grain size dependence on the plot shown in Fig. 9F. On the contrary, Fig. 6C shows a good latitudinal correlation between this proportion of steep slopes, the mean slope, and the [^{10}Be]coarse/[^{10}Be]sand ratio when this ratio is <1. Thus, the distribution of slopes within the catchments seems to control the pattern of deficit for the ^{10}Be concentration in coarse sediment.

4.5. Relationship with the climate

The catchment-mean temperature and precipitation, together with the slope, lithology and vegetation, control the soil thickness and physical weathering. The soil thickness also controls the depth of the landslides, and thus the possible differences between coarse sediment sourced from the deep layers (e.g. Brown et al., 1995) and fine sediment from the surface layers. In addition, water discharge in the rivers controls the rate of downstream size reduction of the cobbles by collision between them. When this process applies to cobbles with a low ^{10}Be concentration (for example because they were exhumed from deep layers of soils by landslides) their collision produces sand with a lower ^{10}Be concentration, which decreases the mean ^{10}Be concentration of the river sand fraction (dilution e.g. Belmont et al., 2007; Carretier et al., 2009). Thus, we analyzed the relationship between the catchment-mean temperature, runoff and [^{10}Be]coarse/[^{10}Be]sand ratio. The mean temperature shows some regional anti-correlation (Fig. 6D). Nevertheless, this anti-correlation may be secondary: temperature is strongly determined by the catchment-mean slope, which is the main erosion control, and both variables show some regional correlation with the [^{10}Be]coarse/[^{10}Be]sand ratio. No correlation appears when plotting the temperature and [^{10}Be]coarse/[^{10}Be]sand ratio in Fig. 10A. Latitudinally, no relationship appears with runoff (Fig. 6C). The [^{10}Be]coarse/[^{10}Be]sand ratio is anti-correlated to the runoff when the runoff is >0.4 m/a (and to the south of 34°S). Note, however, that the slope and erosion rates are also anti-correlated to the runoff to the south of 34°S (Pepin et al., 2010; Carretier et al., 2013).

5. Discussion

5.1. Grain size dependent storage in the system

Another explanation for the observed size-dependent ^{10}Be concentration could be the recycling of stored and older sediments (e.g. Wittmann et al., 2009, 2011b, 2011c). Almost all of the sampled rivers are incised within alluvial terraces (e.g. Abbuehl et al., 2011b; Aguilar et al., 2011; Bekaddour et al., 2014; Riquelme et al., 2011; Rodríguez et al., 2013), which provides a certain amount of sediment to the active river by bank erosion. A long residence time in these terraces increases the ^{10}Be concentration in the sediment. Nevertheless, the terraces are usually higher than 10 m above the river (Fig. 4B and F). The lateral erosion of this material and its incorporation into the river sediment should not significantly increase its ^{10}Be concentration. Moreover, the terrace material is composed of mixed sand, gravel and pebbles without any sorting. There is not a higher amount of pebbles in the deep layer of this terrace material, nor is there more gravel at the surface. In central-northern Chile, part of the terrace sediment has a glacial origin, with a potentially small size-dependent difference in the ^{10}Be concentration (Riquelme et al., 2011). Even if terrace sediment represents a significant fraction of the sampled sediment, they would decrease the ^{10}Be concentration in all sediment sizes.

5.2. Statistical representativity, sediment mixing

There can be questions about the uncertainty associated with the average ^{10}Be concentration in each clast population. This average may be strongly biased in three pebble samples containing less than 16 clasts. Despite the low number of pebbles (6 and 15, respectively) in the two Peruvian canyons, Cañete (CAN2-3) and Ocoña (OCO22-23), they show similar ^{10}Be ratios in the ^{10}Be concentration between pebbles and sand. In the Huasco catchment, sample HUA3 contains 15 pebbles, but shows a similar deficit to the other pebble samples of this catchment containing 30–34 pebbles. The regional co-variation indicated by the grey lines in Fig. 6A, B and C suggests that the observed size-dependent ^{10}Be concentration is not random. The gravel samples contain between 30 and 100 clasts; this should provide a better estimate of the mean ^{10}Be concentration, except if, as discussed later, their source area is wider than for the pebbles.

The lack of sediment mixing could be responsible for the variable size-dependent ^{10}Be concentrations (e.g. Binnie et al., 2006; Reinhardt et al., 2007; Yanites et al., 2009; Savi et al., 2014). For example, a granitoid source that is several hundreds of meters away from the sample site may deliver pebbles for which the ^{10}Be concentration over-represents the concentration in granitoid sources that are even further away. All of the studied catchments are large (>1200 km^2). Such large areas should ensure the mixing of distant sources and prevent an over-representation of sediment coming from a near-by source (Yanites et al., 2009). Another possibility is that a significant part of the pebbles gathered in the river mainly come from a neary-by and large landslide where they resided at depth. Although we cautiously sampled to avoid this situation, this possibility cannot be rejected. For example, we note that in the Choapa catchment in Chile (Fig. 3), pebble sample CHO0823G has a slightly higher or similar ^{10}Be concentration than the sand sample, whereas two other pebbles samples taken at several kilometers

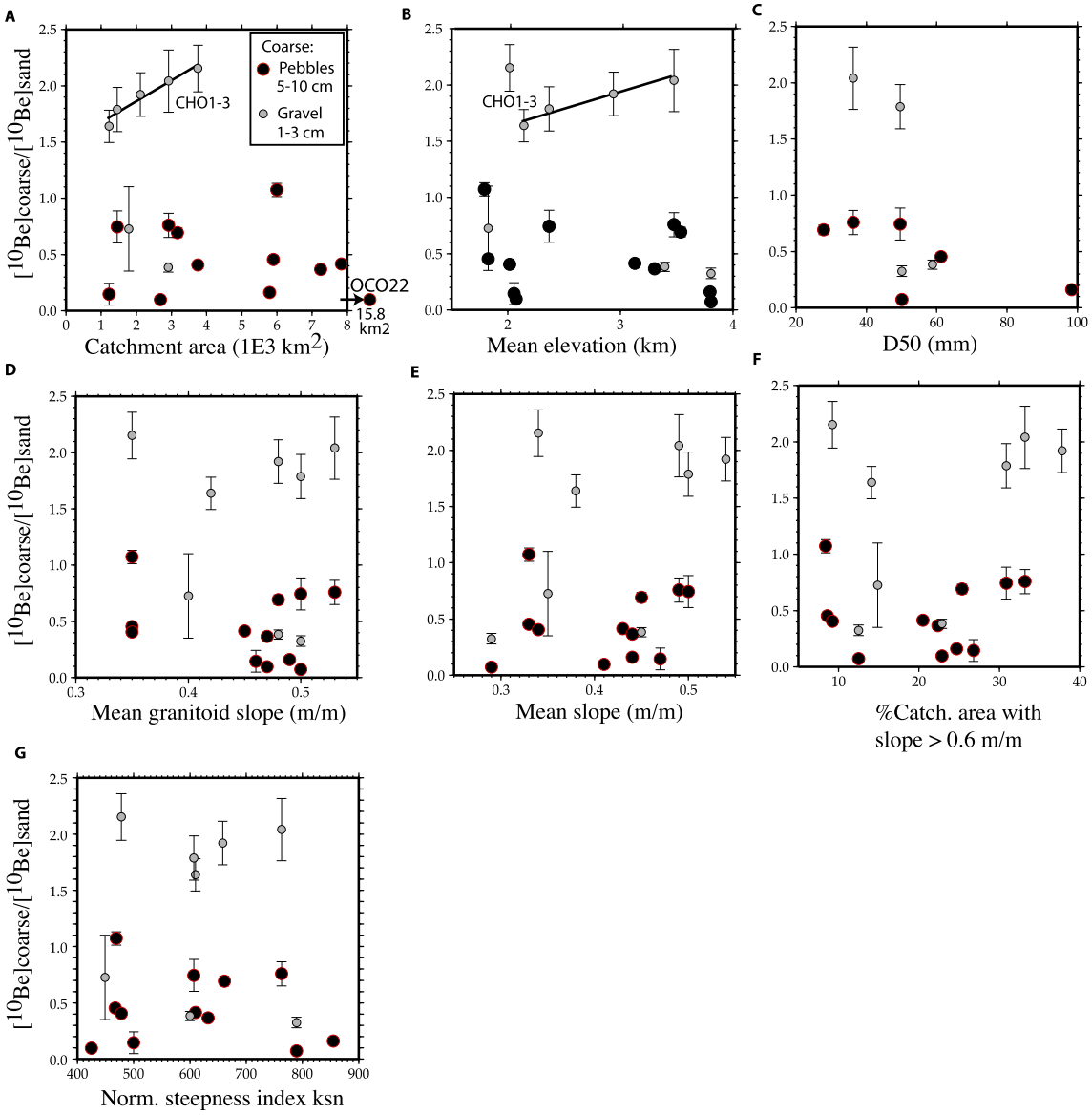

Fig. 9. Relationships between the ^{10}Be concentrations in coarse and sand sediment ([^{10}Be]coarse/[^{10}Be]sand) and geomorphic parameters (see text for details). The sand fraction is [0.5–1] mm.

upstream (CHO0822G and CHO2 – Fig. 3) in the same river have half the ^{10}Be concentration in sand. The Choapa River is incising within a paleo-valley partially filled by sediment from the Confluencia formation, assigned to the Pliocene (Rodríguez et al., 2013). These sediments may include pebbles with variable inherited ^{10}Be concentrations. Their addition to the river bedload may explain the different ^{10}Be concentrations for the Choapa pebble clusters. On the contrary, the corresponding ^{10}Be concentration in sand is similar within uncertainty in the three cases (cf Table 1).

5.3. Hillslope residence in the different layers, mass wasting and heterogeneous erosion rates

Several authors have proposed that large clasts come from the deep layers of landslides (low ^{10}Be production rate) while sand may be produced preferentially in the surface layer of the hillslopes (high ^{10}Be production rate) (e.g. Brown et al., 1995; Belmont et al., 2007; Puchol et al., 2014). A simple calculation can be used to test for this possibility in order to explain the observed [^{10}Be]coarse/[^{10}Be]sand ratios. The ^{10}Be production rate by spallation obeys $P \sim P_o e^{-z/0.6}$, where P_o is the ^{10}Be production rate at the Earth's surface, z is the depth in meters and 0.6 is an estimate for the attenuation length of the neutrons in meters. Using an end-member model where the landslides are composed of two layers (a surface layer of thickness H_s made of sand overlying a layer of thickness H_p made of pebbles) we can calculate a mean ^{10}Be production rate for the two layers. These production rates are:

$$P_s = \frac{1}{H_s}\int_0^{H_s} P dz = \frac{0.6}{H_s}\left[1 - e^{-H_s/0.6}\right]$$

and

$$P_p = \frac{1}{H_p}\int_{H_s}^{H_s+H_p} P dz = \frac{0.6}{H_p}\left[e^{-H_s/0.6} - e^{-(H_s+H_p)/0.6}\right]$$

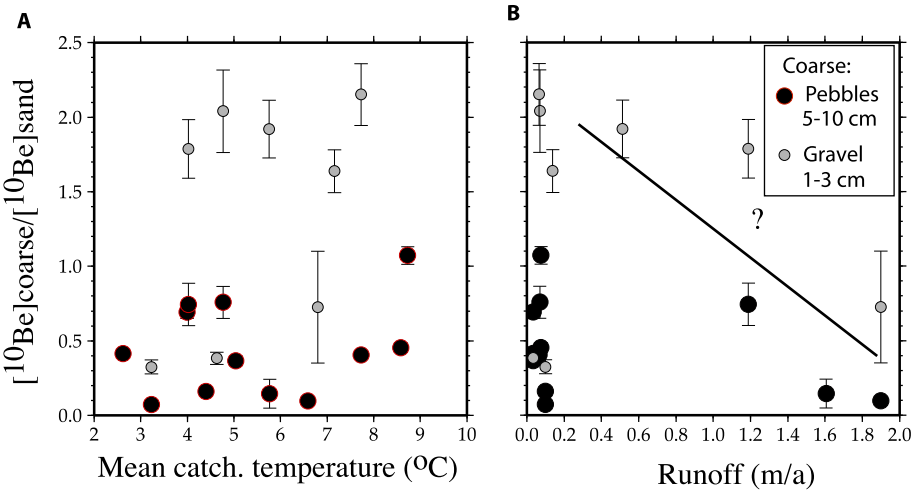

Fig. 10. Relationships between the ^{10}Be concentrations in coarse and sand sediment ([^{10}Be]coarse/[^{10}Be]sand) and catchment-mean temperature and runoff. The sand fraction is [0.5–1] mm.

respectively. With H_s and H_p values ranging between 0.2 m and 1.0 m, P_p/P_s ranges between 0.18 and 0.57. This value increases if sand is also present in the deep layer. This ratio is consistent with the observed [^{10}Be]pebble/[^{10}Be]sand ratio, suggesting that relatively shallow landslides (1–2 m) may produce the observed low [^{10}Be]coarse/[^{10}Be]sand ratios. Mass wasting exists in the studied catchments, which all have steep slopes (e.g. Aguilar et al., 2011; Antinao and Gosse, 2009). It also occurs in the Huasco catchment (Aguilar et al., 2014), and many steep hillslopes of the arid catchment (north of 34°) are covered by mobile soils that are more than 1 m deep, in particular above ~ 2000 m where the physical weathering is more efficient. However, we have no evidence of grain-size sorting in these soils. Locally, we were able to observe thick (1–5 m) saprolite covered by 1–2 m mobile soils even in the arid Maipo catchment (not sampled for this study but located at 34°S east of Santiago – Fig. 3). Cobbles are present at the base of the saprolite. Any landslide affecting the whole regolith would deliver cobbles with low ^{10}Be concentrations to the river (Puchol et al., 2014). Thick saprolites are more likely in the southern and wetter catchments (south of 34°S) where denudation rates decrease southward (Carretier et al., 2013). Yet the deficit of the ^{10}Be concentration in pebbles and gravel compared to sand in these catchments is not larger than in the drier catchments. The southern catchments have smaller slopes (Fig. 6) and denser vegetation, which may prevent mass wasting (Vanacker et al., 2007a,b).

Nevertheless, if the grain size layering in the landslides was the main reason for the observed lower ^{10}Be concentration in gravel and pebbles, we should observe that the deficit of the ^{10}Be concentration in these coarse sediments should increase with the proportion of the catchment area affected by landslides. We would expect that this deficit increases with the catchment slope or with the proportion of steep slopes >0.6 m/m prone to mass wasting. Fig. 9D to F do not show this relationship and the regional variations of these parameters suggest the contrary (Fig. 6B).

A hillslope steepness effect appears when analyzing the contribution of steep granitoid to the catchment-mean ^{10}Be production rate in Fig. 7D. When the contribution of the steep granitoid to the catchment ^{10}Be production rate is larger, the ^{10}Be concentration in sand and coarse sediment with low ^{10}Be concentrations is closer together. A scenario suggested by Aguilar et al. (2014) explains this: it assumes that pebbles are preferentially delivered by steep slopes, dominated by mass wasting, and have higher erosion rates. When steep and fast eroding slopes contribute to a small fraction of the ^{10}Be flux, the ^{10}Be concentration in pebbles is low and that of sand is higher because sand is also derived from areas that erode more slowly (Fig. 1). When steep and fast eroding slopes contribute to a large proportion of the ^{10}Be concentration, pebbles as well as sand have a low and similar ^{10}Be concentration. In this scenario, it is mainly the sand ^{10}Be concentration that makes the difference. The broad regional co-variation of the ^{10}Be concentration deficit in the coarse sediment, erosion rate, catchment slope and proportion of steep slopes supports this interpretation (Fig. 6). This correlation suggests that the transient stage of the catchments, and thus the degree of heterogeneity in their erosion rate, controls the grain size dependence of the ^{10}Be concentration. This interpretation may explain the small difference between sand and coarse sediment in the steep catchments in Tibet (Ouimet et al., 2009; Palumbo et al., 2010), the Alps (Norton et al., 2008; Wittmann et al., 2007) or Ecuadorian Andes (Vanacker et al., 2007a,b). In these catchments, the erosion rate is probably much more homogeneous than in the studied Andes, which are all transient catchments with probable heterogeneous erosion rates (Rehak et al., 2010; Trauerstein et al., 2013). On the other hand, Puchol et al. (2014) showed that gravel ([0.47–4] cm) systematically have a lower ^{10}Be concentration than fine sand within a small Himalayan catchment dominated by mass-wasting. In this particularly humid catchment, pebbles may preferentially come from the deep part of a thick regolith. Climate may control the difference between sand and pebbles in this case. It may be argued that if the relationship with erosion heterogeneity was broadly true, we should observe a better correlation between the mean catchment slope and the ^{10}Be concentration ratios between sand and coarser sediment found in the literature (e.g. Fig. 2B and C). Nevertheless, the mean catchment slope may be not sufficient to determine the degree of erosion rate homogeneity within a catchment. Slope is not the only parameter controlling erosion; lithology, precipitation, vegetation also influence erosion. In order to fully validate our interpretation, at least in our semiarid to mediteranean catchments, it should be proved that 1 – the pebbles are mainly derived from steep catchment areas with higher erosion rates, and 2 – the deficit in the ^{10}Be concentration in coarse sediment increases with the degree of erosion rate heterogeneity within a catchment. This requires additional research in order to be able to map the erosion rates within the studied catchments.

5.4. Long river transport and abrasion

We first discuss the samples with a lower ^{10}Be concentration in pebbles and gravel, and then the five samples with a higher ^{10}Be concentration in gravel.

The downstream fining of sediment by size reduction (attrition) can decrease the mean ^{10}Be concentration in coarse sediment via two phenomena. First, pebbles and gravels produced at high elevations can be crushed into sand, so that the pebbles gathered at the river outlet come mainly from the low elevations of the catchment (see an example and the discusson in Matmon et al., 2003; Belmont et al., 2007) (Fig. 1D). If the erosion rate is homogeneous within a catchment, these pebbles have, on average, a lower ^{10}Be concentration than sand, which can come from everywhere, including high elevations. However, the pebbles gathered along the Huasco River (South latitudes 28.6, 28.7, 28.8, 28.99 in Table 1) display a constant ^{10}Be concentration, which seems to contradict this interpretation. For the other samples, some indications can be derived from Steinberg's attrition law $R = R_o\, e^{-(k/3)x}$ where k (%/km) is the attrition rate, x (km) is the downstream distance and R_o is the initial clast radius (e.g. Attal and Lave, 2006). Attal and Lave (2009) estimated k = 0.4%/km for granite pebbles. Using this k value, an initial pebble with a 5 cm radius (the maximum size of the sampled pebbles) is reduced to sand (R < 2 mm) after a travel distance >2400 km (>1500 km for initial gravel with a 3 cm initial radus). These values are much larger than the studied river length of ~ 100 km, and thus, the complete conversion of granite pebbles and gravel into sand seems unlikely in the studied rivers. Nevertheless, in situ weathering of pebbles could increase the k value (Jones and Humphrey, 1997), which remains to be quantified.

The second phenomenon associated with attrition concerns the size reduction of initially big cobbles or boulders moving in a thick regolith on the hillslopes, as explained by Aguilar et al. (2014). This process requires regolith thicker than 10 m and initial boulders larger than 1 m in diameter. We did not directly observe 10 m thick regolith in our studied steep catchments. Nevertheless, regolith covering hillslopes is common in the studied catchments and such thicknesses might be reached near the bottom of the hillslopes (Fig. 4C and D). Moreover, the reduction of an initial 1 m boulder into a 10 cm pebble in 100 km requires an attrition rate k of 7%/km, which is 17 times larger than the experimental value for granite (Attal and Lave, 2009). This process is thus unlikely to explain the observed differences.

The higher ^{10}Be concentration in the five gravel samples can be explained by a combination of preferential production at high elevations, pebbles breaking in the river, and long river transport. The gravel may correspond to the typical clast size produced by gelifraction at high elevations, where the ^{10}Be production rate is high. Alternatively, gravel may derive from the breaking of larger pebbles also produced at high elevations at the catchment head and which eroded during a long river transport (Attal and Lave, 2009). If these gravel stay for a long period of time in the river, this may even increase their ^{10}Be concentration (Carretier et al., 2009; Yanites et al., 2009). Three arguments support this interpretation. First, the fluvial relief of the studied catchments can reach up to 2.78 km. The ^{10}Be production rate at the catchment head is therefore approximately about three times larger than at the catchment outlet. Second, Fig. 9B shows that the excess in the ^{10}Be concentration in gravel increases with the mean catchment elevation. This suggests that gravel preferentially come from high elevations. CHO1 is an exception; however it is consistent with the third argument: Fig. 9A shows that the excess in the ^{10}Be concentration in gravel is also correlated with the catchment area. A larger area may increase the gravel residence time in the rivers.

Finally, the observed differences between pebbles and gravel might possibly be explained by the different processes that result in these two particular sediment sizes. Pebbles measuring ~5–10 cm might only be derived from fast-eroding hillsopes, where landslides are efficient and pebbles represent the characteristic size of clasts detached from poorly weathered bedrock. Smaller 1–3 cm pieces of gravel may result from a larger number of processes: gelifraction at

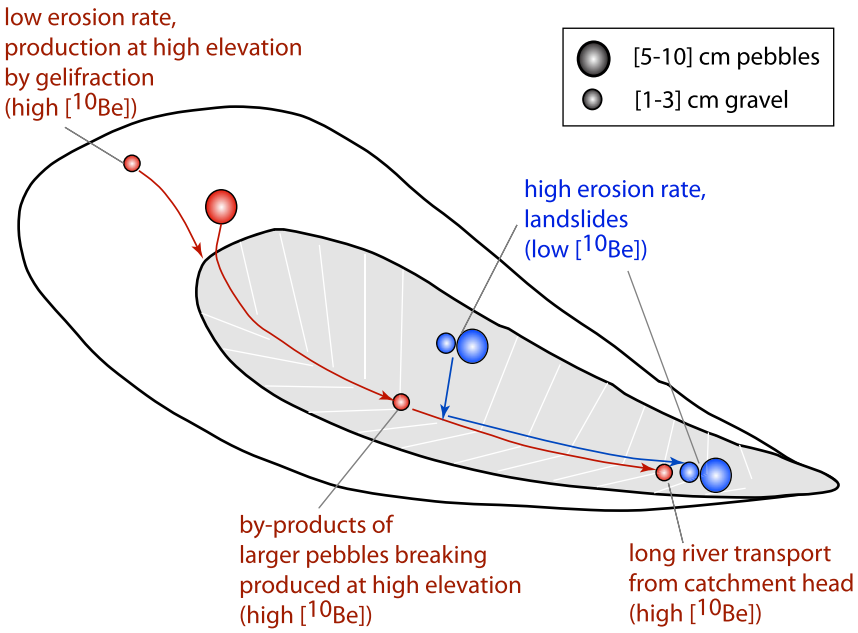

Fig. 11. One possible model for the studied catchments explaining the lower ^{10}Be concentration observed in pebbles and the lower or higher ^{10}Be concentration in gravel. Sand comes from everywhere. Pebbles (5–10 cm) may primarily come from areas with higher erosion rates, such that their ^{10}Be concentration is lower than that of sand on average. Gravel (1–3 cm) may correspond to a typical grain size produced by physical weathering at high elevation, or by the breaking of larger pebbles produced at high elevations during a long river transport. These different sources result in lower or higher ^{10}Be concentrations on average compared to sand. The full demonstration of this model requires further work.

high elevations (high ^{10}Beproduction rate), other physical weathering processes at lower elevations or landslides (low ^{10}Be production rate), by-products of pebble abrasion (variable ^{10}Be concentration -Attal and Lave (2009)). Our pebbles may have a smaller ^{10}Be concentration than sand because they mainly derive from fast-eroding hillslopes, whereas small pieces of gravel have smaller or larger ^{10}Be concentrations because they derive from a larger number of processes (Fig. 11). This difference may also explain the diversity of situations found in the literature between sand and small gravel (Fig. 2).

6. Synthesis and conclusion

From the 20 studied sample pairs, the ^{10}Be concentration in only one gravel sample (LON1), and maybe two others (gravel samples OCO25 and pebble sample ELK3) can be explained by the elevation of the granitoid from which these samples are derived. In the other cases, the granitoid hypsometry does not explain the difference between their ^{10}Be concentration and that of sand.

Five gravel samples show a higher ^{10}Be concentration, while 14 gravel (1–3 cm) and pebble (5–10 cm) samples show a lower ^{10}Be concentration, and one pebble sample shows a similar ^{10}Be concentration.

In order to explain the grain-size dependent differences, authors have proposed various processes that are able to 1 – increase or decrease the ^{10}Be concentration in sand (e.g. Belmont et al., 2007; Yanites et al., 2009) and 2 – increase or decrease the ^{10}Be concentration in coarse sediment (e.g. Belmont et al., 2007; Brown et al., 1995; Carretier et al., 2009; Matmon et al., 2003). Complementary to previous studies, we analyzed these differences in the catchments covering a wide range of climates in the Andes. Spatial variations in the climate do not explain the observed differences. The exhumation of pebbles with low ^{10}Be concentrations from the deep layers of landslides is not evidenced by our data. The analysis suggests an explanation involving a heterogeneous erosion rate in the transient catchments, the preferential production of pebbles in their high erosion rate areas, and variable sources of gravel. According to this explanation, pebbles and gravel have a lower ^{10}Be concentration because they are exhumed at a higher rate, possibly by mass wasting. Sand is produced everywhere in a catchment. When only a fraction of the catchment area is affected by high erosion rates, pebbles and gravel have a lower ^{10}Be concentration on average. When the whole catchment erodes at the same rate, pebbles, gravel and sand are derived from the same sources, and their ^{10}Be concentration is more similar. At the same time, the size reduction of the cobbles yields smaller pieces which mix with the river material. If the cobbles come from much higher elevations, the by-products of their erosion during river transport may add gravel with a high ^{10}Be concentration, so that the mean ^{10}Be concentration in gravel becomes higher than that of sand. Gravel may also be preferentially produced by physical weathering at high elevations. Both phenomena and a possible acquisition of ^{10}Be during long river transport in large catchments explain the excess of ^{10}Be concentration in five gravel samples, and the correlation between this excess, the catchment area, and the catchment-mean elevation. In order to verify the model for our catchments, further work should be undertaken to prove that 1 – the pebbles are preferentially derived from high erosion rate areas and 2 – the deficit in the ^{10}Be concentration in coarse sediment increases with the degree of heterogeneity in the erosion rate within a catchment.

Acknowledgements

This study was funded by the Agence Nationale pour la Recherche, project ANDES (ANR-06-JCJC0100), the Institut de Recherche pour le Développement (IRD) and the ECOS-Conycit program (project C11U02). It is also a contribution to the project Fondecyt project N°1121041 and to the LMI COPEDIM. We thank Christiane Cavare-Hester for drawing Fig. 1. We also thank four anonymous reviewers for their help in different versions of this paper. Their detailed reviews improved greatly this paper. Sara Mullin corrected the English.

Appendix A. Supplementary data

Supplementary data related to this article can be found at http://dx.doi.org/10.1016/j.quageo.2014.12.002.

References

Abbuehl, L.M., Norton, K.P., Jansen, J.D., Schlunegger, F., Aldahan, A., Possnert, G., 2011a. Erosion rates and mechanisms of knickzone retreat inferred from ^{10}Be measured across strong climate gradients on the northern and central Andes Western Escarpment. Earth Surf. Proc. Land. 36 (11), 1464–1473.

Abbuehl, L.M., Norton, K.P., Schlunegger, F., Kracht, O., Aldahan, A., Possnertd, G., 2011b. Corrigendum: El Nino forcing on ^{10}Be-based surface denudation rates in the northwestern Peruvian Andes? (vol. 123, pg 257, 2010). Geomorphology 129 (3–4), 417.

Aguilar, G., Carretier, S., Regard, V., Vassallo, R., Riquelme, R., Martinod, J., 2014. Grain size-dependent ^{10}Be concentrations in alluvial stream sediment of the Huasco Valley, a semi-arid Andes region. Quat. Geochronol. 19, 163–172.

Aguilar, G., Riquelme, R., Martinod, J., Darrozes, J., Maire, E., 2011. Variability in erosion rates related to the state of landscape transience in the semi-arid Chilean Andes. Earth Surf. Proc. Land 36 (13), 1736–1748.

Antinao, J., Gosse, J., 2009. Large rockslides in the Southern Central Andes of Chile (32–34.5 degrees S): tectonic control and significance for quaternary landscape evolution. Geomorphology 104, 117–133.

Attal, M., Lave, J., 2006. Changes of bedload characteristics along the Marsyandi river (central Nepal): implications for understanding hillslope sediment supply, sediment load evolution along fluvial networks, and denudation in active orogenic belts. In: Willett, S., Hovius, N., Brandon, M., Fisher, D. (Eds.), Tectonics, Climate, and Landscape Evolution, Geological Society of America Special Paper, vol. 398, pp. 143–171.

Attal, M., Lave, J., 2009. Pebble abrasion during fluvial transport: experimental results and implications for the evolution of the sediment load along rivers. J. Geophys. Res. Earth Surf. 114, F04023.

Baker, S.E., Gosse, J.C., McDonald, E.V., Evenson, E.B., Martinez, O., 2009. Quaternary history of the piedmont reach of Rio Diamante, Argentina. J. South Am. Earth S. C. 28 (1), 54–73.

Balco, G., Stone, J., Lifton, N., Dunai, T., 2008. A complete and easily accessible means of calculating surface exposure ages or erosion rates from ^{10}Be and ^{26}Al measurements. Quat. Geochronol. 3, 174–195.

Bekaddour, T., Schlunegger, F., Vogel, H., Delunel, R., Norton, K.P., Akçar, N., Kubik, P., 2014. Paleo erosion rates and climate shifts recorded by quaternary cut-and-fill sequences in the Pisco valley, central Peru. Earth Planet. Sci. Lett. 390, 103–115.

Belmont, P., Pazzaglia, F., Gosse, J., 2007. Cosmogenic ^{10}Be as a tracer for hillslope and channel sediment dynamics in the Clearwater River, western Washington State. Earth Planet. Sci. Lett. 264, 123–135.

Bierman, P.R., Nichols, K.K., 2004. Rock to sediment-slope to sea with ^{10}Be-rates of landscape change. Annu. Rev. Earth Planet. Sci. 32, 215–255.

Bierman, P.R., Steig, E.J., 1996. Estimating rates of denudation and sediment transport using cosmogenic isotope abundances in sediment. Earth Surf. Proc. Land 21, 125–239.

Binnie, S., Phillips, W., Summerfield, M., Fifield, L., 2006. Sediment mixing and basin-wide cosmogenic nuclide analysis in rapidly eroding mountainous environments. Quat. Geochronol. 1, 4–14.

Binnie, S.A., Phillips, W.M., Summerfield, M.A., Fifield, L.K., 2007. Tectonic uplift, threshold hillslopes, and denudation rates in a developing mountain range. Geology 35 (8), 743–746.

Bissig, T., Clark, A., Lee, J., Hodgson, C., 2002. Miocene landscape evolution and geomorphologic controls on epithermal processes in the El Indio-Pascua Au-Ag-Cu belt, Chile and Argentina. Econ. Geol. Bull. Soc. Econ. Geol. 97 (5), 971–996.

Braucher, R., Bourlès, D., Merchel, S., Romani, J.V., Fernadez-Mosquera, D., Marti, K., Léanni, L., Chauvet, F., Arnold, M., Aumaître, G., Keddadouche, K., 2013. Determination of muon attenuation lengths in depth profiles from in situ produced cosmogenic nuclides. Nucl. Instrum. Methods Phys. Res. 294, 484–490.

Braucher, R., Brown, E., Bourlès, D., Colin, F., 2003. In situ produced ^{10}Be measurements at great depths: implications for production rates by fast muons. Earth Planet. Sci. Lett. 211, 251–258.

Brown, E., Bourlès, D., Burchfiel, B., Deng, Q., Li, J., Molnar, P., Raisbeck, G., Yiou, F., 1998. Estimation of slip rates in the southern Tien Shan using cosmic ray exposure dates of abandoned alluvial fans. Geol. Soc. Am. Bull. 110, 377–386.

Brown, E.T., Stallard, R.F., Larsen, M.C., Raisebeck, G.M., Yiou, F., 1995. Denudation rates determined from the accumulation of in situ-produced ^{10}Be in the Luquillo experimental Forest, Puerto Rico. Earth Planet. Sci. Lett. 129, 193–202.

Carretier, S., Regard, V., 2011. Is it possible to quantify pebble abrasion and velocity in rivers using terrestrial cosmogenic nuclides? J. Geophys. Res. Earth Surf. 116, F04003.

Carretier, S., Regard, V., Soual, C., 2009. Theoretical cosmogenic nuclide concentration in river bedload clasts: does it depend on clast size? Quat. Geochronol. 4, 108–123.

Carretier, S., Regard, V., Vassallo, R., Aguilar, G., Martinod, J., Riquelme, R., Pepin, E., Charrier, R., Hérail, G., Farías, M., Guyot, J.-L., Vargas, G., Lagane, C., 2013. Slope and climate variability control of erosion in the Andes of central Chile. Geology 41 (2), 195–198.

Carretier, S., Tolorza, V., Rodríguez, M., Pepin, E., Aguilar, G., Regard, V., Martinod, J., Riquelme, R., Bonnet, S., Brichau, S., Hérail, G., Pinto, L., Farías, M., Charrier, R., Guyot, J., 2014. Erosion in the Chilean Andes between 27S and 39S: tectonic, climatic and geomorphic control. Geol. Soc. Lond. Special Publ. 399 http://dx.doi.org/10.1144/SP399.16.

Charrier, R., Pinto, L., Rodríguez, M., 2007. Tectono-stratigraphic evolution of the Andean orogen in Chile. In: Gibbons, W., Moreno, T. (Eds.), Geology of Chile. The Geological Society London Special Publication, pp. 21–116.

Clapp, E., Bierman, P., Caffee, M., 2002. Using ^{10}Be and ^{26}Al to determine sediment generation rates and identify sediment source areas in an arid region drainage basin. Geomorphology 45 (1–2), 67–87.

Clapp, E., Bierman, P., Nichols, K., Pavich, M., Caffee, M., 2001. Rates of sediment supply to arroyos from upland erosion determined using in situ produced cosmogenic ^{10}Be and ^{26}Al. Quat. Res. 55, 235–245.

Clapp, E., Bierman, P., Schick, A., Lekach, Y., Enzel, Y., Caffee, M., 2000. Sediment yield exceeds sediment production in arid region drainage basins. Geology 28, 995–998.

Codilean, A., 2006. Calculation of the cosmogenic nuclide production topographic shielding scaling factor for large areas using DEMs. Earth Surf. Proc. Land 31 (6), 785–794.

Codilean, A., Fenton, C., Fabel, D., Bishop, P., Xu, S., 2014. Discordance between cosmogenic nuclide concentrations in amalgamated sands and individual fluvial pebbles in an arid zone catchment. Quat. Geochronol. 19, 173–180.

Codilean, A.T., Bishop, P., Hoey, T.B., Stuart, F.M., Fabel, D., 2010. Cosmogenic ^{21}Ne analysis of individual detrital grains: opportunities and limitations. Earth Surf. Proc. Land 35 (1), 16–27.

Derrieux, F., Siame, L.L., Bourlès, D.L., Chen, R.-F., Braucher, R., Leanni, L., Lee, J.-C., Chu, H.-T., Byrne, T.B., 2014. How fast is the denudation of the Taiwan mountain belt? Perspectives from in situ cosmogenic ^{10}Be. J. Asian Earth Sci. 88, 230–245.

Dunai, T., Lopez, G., Juez-Larre, J., 2005. Oligocene-Miocene age of aridity in the Atacama Desert revealed by exposure dating of erosion-sensitive landforms. Geology 33 (4), 321–324.

Evenstar, L.A., Hartley, A.J., Stuart, F.M., Mather, A.E., Rice, C.M., Chong, G., 2009. Multiphase development of the Atacama Planation surface recorded by cosmogenic ^{3}He exposure ages: implications for uplift and Cenozoic climate change in western South America. Geology 37 (1), 27–30.

Gayer, E., Mukhopadhyay, S., Meade, B., 2008. Spatial variability of erosion rates inferred from the frequency distribution of cosmogenic ^{3}He in olivines from hawaiian river sediments. Earth Planet. Sci. Lett. 266 (3–4), 303–315.

Granger, D., Kircher, J., Finkel, R., 1996. Spatially averaged long-term erosion rates measured from in situ-produced cosmogenic nuclides in alluvial sediment. J. Geol. 104, 249–257.

Hall, S.R., Farber, D.L., Audin, L., Finkel, R.C., Meriaux, A.S., 2008. Geochronology of pediment surfaces in southern Peru: implications for quaternary deformation of the Andean forearc. Tectonophysics 459 (1–4), 186–205, 6th International Symposium on Andean Geodynamics (ISAG), Barcelona, Spain, Sepp. 12–14, 2005.

Heimsath, A.M., Chappell, J., Fifield, K., 2010. Eroding Australia: rates and processes from Bega Valley to Arnhem land. Geol. Soc. Lond. Spec. Publ. 346, 225–241.

Hewawasam, T., von Blanckenburg, F., Schaller, M., Kubik, P., 2003. Increase of human over natural erosion rates in tropical highlands constrained by cosmogenic nuclides. Geology 31 (7), 597–600.

Hippe, K., Kober, F., Zeilinger, G., Ivy-Ochs, S., Maden, C., Wacker, L., Kubik, P.W., Wieler, R., 2012. Quantifying denudation rates and sediment storage on the eastern Altiplano, Bolivia, using cosmogenic ^{10}Be, ^{26}Al, and in situ ^{14}C. Geomorphology 179, 58–70.

Insel, N., Ehlers, T.A., Schaller, M., Barnes, J.B., Tawackoli, S., Poulsen, C.J., 2010. Spatial and temporal variability in denudation across the Bolivian Andes from multiple geochronometers. Geomorphology 122 (1–2), 65–77.

Jones, L., Humphrey, N., 1997. Weathering-controlled abrasion in a coarse-grained, meandering reach of the Rio Grande: implications for the rock record. Geol. Soc. Am. Bull. 109, 1080–1088.

Jungers, M.C., Heimsath, A.M., Amundson, R., Balco, G., Shuster, D., Chong, G., 2013. Active erosion-deposition cycles in the hyperarid Atacama desert of Northern Chile. Earth Planet. Sci. Lett. 371, 125–133.

Kober, F., Ivy-Ochs, S., Schlunegger, F., Baur, H., Kubik, P., Wieleb, R., 2007. Denudation rates and a topography-driven rainfall threshold in northern Chile: multiple cosmogenic nuclide data and sediment yield budgets. Geomorphology 83, 97–120.

Kober, F., Ivy-Ochs, S., Zeilinger, G., Schlunegger, F., Kubik, P., Baur, H., Wieler, R., 2009. Complex multiple cosmogenic nuclide concentration and histories in the arid Rio Lluta catchment, northern Chile. Earth Surf. Proc. Land 34 (3), 479–479.

Lavado, W., Ronchail, J., Labat, D., Espinoza, J., Guyot, J., 2012. Basin-scale analysis of rainfall and runoff in Peru (1969-2004): Pacific, Titicaca and Amazonas drainages. Hydrol. Sci. J. 57 (4), 625–642.

Matmon, A., Bierman, P., Larsen, J., Southworth, S., Pavich, M., Finkel, R., Caffee, M., 2003. Erosion of an ancient mountain range, the Great Smoky Mountains, north Carolina and Tennessee. Am.. J. Sci. 303, 817–855.

Matmon, A., Bierman, P., Larsen, J., Southworth, S., Pavich, M., Finkel, R., Caffee, M., 2005a. Grain size dependency of ^{10}Be concentrations in alluvial sediments in the Great Smoky mountains. Geochim. Cosmochim. Acta 69 (Suppl. l), A160.

Matmon, A., Schwartz, D., Finkel, R., Clemmens, S., Hanks, T., 2005b. Dating offset fans along the Mojave section of the San Andreas fault using cosmogenic ^{26}Al and ^{10}Be. Geol. Soc. Am. Bull. 117, 795–807.

Matmon, A., Mushkin, A., Enzel, Y., Grodek, T., Team, A.S.T.E.R., 2013. Erosion of a granite inselberg, Gross Spitzkoppe, Namib desert. Geomorphology 201, 52–59.

McPhillips, D., Bierman, P.R., Crocker, T., Rood, D.H., 2013. Landscape response to Pleistocene-Holocene precipitation change in the Western Cordillera, Peru: ^{10}Be concentrations in modern sediments and terrace fills. J. Geophys. Res. Earth Surf. 118 (4), 2488–2499.

Melnick, D., Bookhagen, B., Strecker, M.R., Echtler, H.P., 2009. Segmentation of megathrust rupture zones from fore-arc deformation patterns over hundreds to millions of years, Arauco peninsula, Chile. J. Geophys. Res. Earth Surf. 114, B01407.

Nichols, K.K., Bierman, P.R., Hooke, R., Caffee, M.W., C, E.M., 2002. Quantifying sediment transport on desert piedmonts using ^{10}Be and ^{26}Al. Geomorphology 45 (2), 105–125.

Niemi, N., Oskin, M., Burbank, D., Heimsath, A., Gabet, E., 2005. Effects of bedrock landslides on cosmogenically determined erosion rates. Earth Planet. Sci. Lett. 237, 480–498.

Nishiizumi, K., Caffee, M., Finkel, R., Brimhall, G., Motel, T., 2005. Remnants of a fossil alluvial fan landscape of Miocene age in the Atacama Desert of northern Chile using cosmogenic nuclide exposure age dating. Earth Surf. Proc. Land 237, 499–507.

Nishiizumi, K., Imamura, M., Caffee, M., Southon, J., Finkel, R., McAnich, J., 2007. Absolute calibration of ^{10}Be AMS standards. Nuclear instruments and methods. Phys. Res. 258, 403–413.

Norton, K.P., von Blanckenburg, F., DiBiase, R., Schlunegger, F., Kubik, P.W., 2011. Cosmogenic ^{10}Be-derived denudation rates of the Eastern and Southern European Alps. Int. J. Earth Sci. 100 (5), 1163–1179.

Norton, K.P., von Blanckenburg, F., Schlunegger, F., Schwab, M., Kubik, P.W., 2008. Cosmogenic nuclide-based investigation of spatial erosion and hillslope channel coupling in the transient foreland of the Swiss Alps. Geomorphology 95 (3–4), 474–486.

Oskin, M., Perg, L., Shelef, E., Strane, M., Gurney, E., Singer, B., Zhang, X., 2008. Elevated shear zone loading rate during an earthquake cluster in eastern California. Geology 36, 507–510.

Ouimet, W.B., Whipple, K.X., Granger, D.E., 2009. Beyond threshold hillslopes: channel adjustment to base-level fall in tectonically active mountain ranges. Geology 37 (7), 579–582.

Palumbo, L., Hetzel, R., Tao, M., Li, X., 2010. Topographic and lithologic control on catchment-wide denudation rates derived from cosmogenic ^{10}Be in two mountain ranges at the margin of NE Tibet. Geomorphology 117 (1–2), 130–142.

Pepin, E., Carretier, S., Guyot, J., Escobar, F., 2010. Specific suspended sediment yields of the Andean rivers of Chile and their relationship to climate, slope and vegetation. Hydrol. Sci. J. 55 (7), 1190–1205.

Pepin, E., Carretier, S., Hérail, G., Regard, V., Charrier, R., Farìas, M., Garcìa, V., Giambiagi, L., 2013. Pleistocene landscape entrenchment: a geomorphological mountain to foreland field case, the Las Tunas system, Argentina. Basin Res. 25, 1–25.

Puchol, N., Lavé, J., Lupker, M., Blard, P., Gallo, F., France-Lanord, C., ASTER-Team1, 2014. Grain-size dependent concentration of cosmogenic ^{10}Be and erosion dynamics in a landslide-dominated Himalayan watershed. Geomorphology 224, 55–68.

Quezada, J., Gonzalez, G., Dunai, T., Jensen, A., Juez-Larre, J., 2007. Pleistocene littoral uplift of northern Chile: ^{21}Ne age of the upper marine terrace of Caldera-Bahia Inglesa area. Rev. Geol. Chile 34 (1), 81–96.

Rehak, K., Bookhagen, B., Strecker, M., Echtler, H.P., 2010. The topographic imprint of a transient climate episode: the western Andean flank between 15.5 and 41.5S. Earth Surf. Proc. Land 35 (13), 1516–1534.

Reinhardt, L., Hoey, T., Barrows, T., Dempster, T., Bishop, P., Fifield, L., 2007. Interpreting erosion rates from cosmogenic radionuclide concentrations measured in rapidly eroding terrain. Earth Surf. Process. Landf. 32, 390–406.

Riquelme, R., Rojas, C., Aguilar, G., Flores, P., 2011. Late pleistocene-early holocene paraglacial and fluvial sediment history in the Turbio valley, semiarid Chilean Andes. Quat. Res. 75 (1), 166–175.

Rodríguez, M., Carretier, S., Charrier, R., Saillard, M., Regard, V., Hérail, G., Hall, S., Farber, D., Audin, L., 2013. Geochronology of pediments and marine terraces in north-central Chile and their implications for quaternary uplift in the Western Andes. Geomorphology 180-181, 33–46.

Roering, J.J., Kirchner, J.W., Dietrich, W.E., 1999. Evidence for nonlinear, diffusive sediment transport on hillslopes and implications for landscape morphology. Water Resour. Res. 35, 853–870.

Safran, E., Bierman, P., Aalto, R., Dunne, T., Whipple, K., Caffee, M., 2005. Erosion rates driven by channel network incision in the Bolivian Andes. Earth Surf. Proc. Land 30, 1007–1024.

Saillard, M., Hall, S.R., Audin, L., Farber, D.L., Hérail, G., Martinod, J., Regard, V., Finkel, R.C., Bondoux, F., 2009. Non-steady long-term uplift rates and pleistocene marine terrace development along the Andean margin of Chile (31 degrees S) inferred from ^{10}Be dating. Earth Planet. Sci. Lett. 277 (1–2), 50–63.

Saillard, M., Hall, S.R., Audin, L., Farber, D.L., Regard, V., Herail, G., 2011. Andean coastal uplift and active tectonics in southern Peru: ^{10}Be surface exposure dating of differentially uplifted marine terrace sequences (San Juan de Marcona, similar to 15.4 degrees S). Geomorphology 128 (3–4), 178–190.

Savi, S., Norton, K., Picotti, V., Brardinoni, F., Akcar, N., Kubik, P., Delunel, R., Schlunegger, F., 2014. Effects of sediment mixing on ^{10}Be concentrations in the Zielbach catchment, central-eastern Italian Alps. Quat. Geochronol. 19, 148–162.

Schaller, M., von Blanckenburg, F., Hovius, N., Kubik, P., 2001. Large-scale erosion rates from in situ-produced cosmogenic nuclides in european river sediments. Earth Planet. Sci. Lett. 188, 441–458.

Schildgen, T., Hodges, K., Whipple, K., Reiners, P., Pringle, M., 2007. Uplift of the western margin of the Andean plateau revealed from canyon incision history, southern Peru. Geology 35, 523–526.

Steffen, D., Schlunegger, F., Preusser, F., 2009. Drainage basin response to climate change in the Pisco valley, Peru. Geology 37, 491–494.

Stock, G.M., Frankel, K.L., Ehlers, T.A., Schaller, M., Briggs, S.M., Finkel, R.C., 2009. Spatial and temporal variations in denudation of the Wasatch Mountains, Utah, USA. Lithosphere 1 (1), 34–40.

Stone, J., 2000. Air pressure and cosmogenic isotope production. J. Geophys. Res. 105, 23753–23759.

Thouret, J.-C., Worner, G., Gunnell, Y., Singer, B., Zhang, X., Souriot, T., 2007. Geochronologic and stratigraphic constraints on canyon incision and Miocene uplift of the Central Andes in Peru. Earth Planet. Sci. Lett. 263, 151–166.

Trauerstein, M., Norton, K.P., Preusser, F., Schlunegger, F., 2013. Climatic imprint on landscape morphology in the western escarpment of the Andes. Geomorphology 194, 76–83.

Vanacker, V., Molina, A., Govers, G., Poesen, J., Deckers, J., 2007a. Spatial variation of suspended sediment concentrations in a tropical Andean river system: the Paute River, southern Ecuador. Geomorphology 87, 53–67.

Vanacker, V., von Blanckenburg, F., Govers, G., Molina, A., Poesen, J., Deckers, J., Kubik, P., 2007b. Restoring dense vegetation can slow mountain erosion to near natural benchmark levels. Geology 35 (4), 303–306.

von Blanckenburg, F., 2005. The control mechanisms of erosion and weathering at basin scale from cosmogenic nuclides in river sediment. Earth Planet. Sci. Lett. 237, 462–479.

von Blanckenburg, F., Belshaw, N., O'Nions, R., 1996. Separation of ^{10}Be and cosmogenic ^{10}Be from environmental materials and SIMS isotope dilution analysis. Chem. Geol. 129, 93–99.

Walcek, A., Hoke, G., 2012. Surface uplift and erosion of the southernmost Argentine Precordillera. Geomorphology 153–154, 156–168.

Wittmann, H., von Blanckenburg, F., Guyot, J.-L., Laraque, A., Bernal, C., Kubik, P.W., 2011a. Sediment production and transport from in situ-produced cosmogenic ^{10}Be and river loads in the Napo River basin, an upper Amazon tributary of Ecuador and Peru. J. South. Am. Earth Sci. 31 (1), 45–53.

Wittmann, H., von Blanckenburg, F., Guyot, J.-L., Maurice, L., Kubik, P.W., 2009. From source to sink: preserving the cosmogenic ^{10}Be-derived denudation rate signal of the Bolivian Andes in sediment of the Beni and Mamore foreland basins. Earth Planet. Sci. Lett. 288 (3–4), 463–474.

Wittmann, H., von Blanckenburg, F., Kruesmann, T., Norton, K.P., Kubik, P.W., 2007. Relation between rock uplift and denudation from cosmogenic nuclides in river sediment in the Central Alps of Switzerland. J. Geophys. Res. Earth Surf. 112, (F4).

Wittmann, H., von Blanckenburg, F., Maurice, L., Guyot, J.-L., Filizola, N., Kubik, P.W., 2011b. Sediment production and delivery in the Amazon River basin quantified by in situ-produced cosmogenic nuclides and recent river loads. Geol. Soc. Am. Bull. 123 (5–6), 934–950.

Wittmann, H., von Blanckenburg, F., Maurice, L., Guyot, J.-L., Kubik, P.W., 2011c. Recycling of Amazon floodplain sediment quantified by cosmogenic ^{26}Al and ^{10}Be. Geology 39 (5), 467–470.

Wittmann, H., VonBlanckenburg, F., 2009. Cosmogenic nuclide budgeting of floodplain sediment transfer. Geomorphology 109, 246–256.

Wobus, C., Whipple, K., Kirby, E., Snyder, N., Johnson, J., Spyropolou, K., Crosby, B., Sheehan, D., 2006. Tectonics from topography: procedures, promise, and pitfalls. In: Willett, S., Hovius, N., Brandon, M., Fisher, D. (Eds.), Tectonics, Climate, and Landscape Evolution, Geological Society of America Special Paper, vol. 398, pp. 55–74.

Yanites, B., Tucker, G., Anderson, R., 2009. Numerical and analytical models of cosmogenic radionuclide dynamics in landslide-dominated drainage basins. J. Geophys. Res. 114, F01007.